Midlatitude lightning NO_x production efficiency inferred from OMI and WWLLN data

Eric Bucsela[1]

Kenneth E. Pickering[2]

Dale Allen[2]

Robert Holzworth[3]

Nickolay Krotkov[4]

[1] SRI International, Menlo Park, CA

[2] Dept. of Atmospheric and Oceanic Science, University of Maryland, College Park, MD

[3] Dept. of Earth and Space Sciences, University of Washington, Seattle, WA

[4] Atmospheric Chemistry and Dynamics Laboratory, NASA Goddard Space Flight Center, Greenbelt, MD

Key Points:

- Lightning flash rates from the World Wide Lightning Location Network are distinctly correlated with lightning-NO_x estimates from the Ozone Monitoring Instrument.

- The observations yield a mean midlatitude production efficiency (PE) of 180 ± 100 moles of lightning NO_x (LNO_x) per lightning flash.

- LNO_x production is proportional to a power function of lightning flash rate, with exponent < 1. Results imply that the PE is lower in storms with more frequent flashes.

Abstract

Oxides of nitrogen are critical trace gases in the troposphere and are precursors for nitrate aerosol and ozone, which is an important pollutant and greenhouse gas. Lightning is the major source of NO_x (NO + NO_2) in the mid- to upper troposphere. We estimate the production efficiency (PE) of lightning NO_x (LNO_x) using satellite data from the Ozone Monitoring Instrument (OMI) and the ground-based World Wide Lightning Location Network (WWLLN) in three northern midlatitude, primarily continental regions that include much of North America, Europe and East Asia. Data were obtained over 5 boreal summers, 2007 – 2011 and comprise the largest number of midlatitude convective events to date for estimating the LNO_x PE with satellite NO_2 and ground-based lightning measurements. In contrast to some previous studies, the algorithm assumes no minimum flash-rate threshold and estimates freshly produced LNO_x by subtracting a background of aged NO_x estimated from the OMI dataset itself. We infer an average value of 180 ± 100 moles LNO_x produced per lightning flash. We also show evidence of a dependence of PE on lightning flash rate and find an approximate empirical power function relating moles LNO_x to flashes. PE decreases by an order of magnitude for a 2-order of magnitude increase in flash rate. This phenomenon has not been reported in previous satellite

LNO_x studies but is consistent with ground-based observations suggesting an inverse relationship between flash rate and size.

Plain-language summary:

Oxides of nitrogen (NO_x = NO + NO_2) are minor gases in the atmosphere but are important in its chemistry. Their major source in the upper troposphere is lightning, which creates nitric oxide (NO) by breaking apart nitrogen and oxygen molecules. Estimating how much total NO is produced requires knowledge of the average production efficiency (PE) of individual lightning flashes. From midlatitude satellite measurements of nitrogen dioxide (NO_2) and lightning detections from ground, we find a mean PE of 175 moles NO per lightning flash, somewhat smaller than the ~250 mol per flash averaged globally in previous studies. We also show that PE is smaller in storms with more frequent lightning.

Keywords:

Lightning, NO_x production, Satellite, OMI, WWLLN

1. Introduction

Trace gases individually represent less than 1% of all components of the earth's atmosphere, but play significant roles in atmospheric chemistry. In particular, nitric oxide (NO) and nitrogen dioxide (NO_2), collectively NO_x, are critical in regulating concentrations of other trace gases. In pollution-free regions, the total NO_x column is dominated by the stratospheric component. There, NO_x occurs naturally as a byproduct of photo-dissociation of N_2O transported across the tropopause and plays a major role in the catalytic destruction of stratospheric ozone (Seinfeld & Pandis, 1998; Finlayson-Pitts & Pitts, 2000). Significant amounts of NO_x also exist in the troposphere with global production estimates of ~48 Tg N/yr (Miyazaki et al., 2016). Tropospheric NO_x is generated by high-temperature reactions involving N_2 and O_2. These are mainly anthropogenic and include combustion of fossil fuels and biomass burning. On average, some 90% of tropospheric NO_x resides in the boundary layer, where it is a precursor to lower-tropospheric ozone. Ground-level NO_2 considered a criteria pollutant.

The major natural source of tropospheric NO_x is lightning (Seinfeld and Pandis, 1998; Finlayson-Pitts and Pitts, 2000). It is estimated that lightning NO_x (LNO_x) accounts for 60-70% of NO_x in the free troposphere (Allen et al., 2010). In the mid-upper troposphere, lightning dissociates N_2 and O_2, into free N and O within the extremely hot flash channel. These in turn react with ambient N_2 and O_2 to produce NO, which remains after the lightning channel cools. During the conversion between NO and NO_2, ozone is generated in the presence of HO_2 and organic peroxy radicals, collectively called RO_2. Ozone is a significant greenhouse gas in the upper troposphere (e.g. Rap et al., 2015). It is sensitive to LNO_x amounts, which are believed to be responsible for 35-45% of global free-tropospheric ozone (Allen et al., 2010; Dahlmann et al. 2011; Liaskos et al., 2015). Pickering et al. (1993, 1996) have shown persistent ozone enhancements downwind of convection. These long-range enhancements are consistent with NO_x lifetimes of at least 2-3 days in the upper troposphere (Jaeglé et al., 1998, Schumann and Huntrieser, 2007; Martin et al., 2007), although initial lifetimes near the lightning source have been shown to be as short as 2-12 hours (Nault et al. 2017). In addition to its direct effect on radiative forcing, ozone can photodissociate and react with water vapor to create hydroxyl (OH), a strong oxidant. Among other roles, OH plays a large role in the destruction of methane (CH_4), another major greenhouse gas (Seinfeld and Pandis, 1998; Finlayson-Pitts and Pitts, 2000; Labrador et al. 2004; DeCaria, 2000, 2005; Fiore et al., 2006; Liaskos et al. 2015).

Production rates of LNO_x depend, in part, on lightning flash rates, and knowledge of these rates is critical in developing chemical transport models (CTMs). On the mesoscale, flash rates have been shown to vary as a power function of cloud-top height (Williams et al., 1985; Price and Rind, 1992). Modeling studies have employed CTM flash parameterizations based on cloud-top-height, convective precipitation rate, anvil-level ice amounts and vertical mass transport in updrafts (Tost et al., 2007; Allen et al., 2010). Murray et al. (2012) showed that flash rates in CTMs may be constrained with satellite measurements of lightning. Globally, mean annual flash rates are estimated to be approximately 46 flashes per second (e.g. Cecil et al., 2014).

Lightning NO_x production estimates also require knowledge of the moles of NO_x produced per flash known as the production efficiency (PE). This quantity is considerably less well known than the global flash rate. Schumann & Huntrieser (2007) cite previous studies of PE spanning ~3 orders of magnitude from ~5 to > 1000 mol per flash. PE values estimated from theory include Bhetanabhotla et al. (1985) (27 mol per flash), Kumar et al. (1995) (100 mol per flash) and Price et al. (1997) (110 to 1100 mol per flash). The theoretical values generally distinguish between cloud-to-ground (CG) and intracloud (IC) flashes. Price et al. (1997) estimated that CG flashes have PE values an order of magnitude higher than those of IC flashes. Koshak (2014) combined observations of lightning channel lengths with theoretical and laboratory NO production estimates, yielding 604 and 38 mol per flash for CG and IC flashes, respectively. Laboratory studies yielding smaller PEs include Wang et al. (1998) (103 mol per flash), Cook et al., (2000) (7 to 120 mol per flash) and Peyrous and Lapeyre (1982) (47 mol per flash). Aircraft observations in conjunction with cloud-scale models suggest that IC and CG flashes are ~equally productive (DeCaria et al., 2005; Ott et al., 2007, 2010; Huntrieser et al., 2011; Cummings et al., 2013). Examples of aircraft/model values are DeCaria et al. (2005) (350 to 470 mol per flash), Ott et al. (2007) (360 mol per flash), Ott et al., (2010) (500 to 700 mol per flash), Huntrieser et al., (2011) (70 to 179 mol per flash) and Cummings et al. (2013) (500 to 600 mol per flash).

Uncertainty in the PE leads to considerable uncertainty in the global LNO_x budget and in CTM parameterizations. Schumann & Huntrieser (2007) suggest a global average PE of 250 mol per flash, which when coupled with the mean annual flash rate yields a global production of 5 ± 3 Tg N/yr when uncertainties are included. Most CTMs assume PEs of 250 – 500 mol per flash, which have been shown in some studies to best reconcile large-scale computed NO_x fields with observations (Martin et al., 2007; Hudman et al., 2007; Allen et al., 2010, 2012). Nault et al. (2017) showed best agreement between models and measurements with a relatively high value of

665 mol per flash. Some studies have suggested midlatitude flashes are more productive than those in tropical regions (Huntrieser et al., 2006; Hudman et al., 2007; Huntrieser et al., 2008). The Goddard Earth Observing System Chemistry (GEOS-Chem) (van Donkelaar et al., 2008) and Global Modeling Initiative (GMI) CTMs (Allen et al., 2010) assume midlatitude PE is twice that in the tropics. Differences between continental and marine flash productivity may also exist. Allen et al. (2019) found marine flashes were two to four times more productive than continental flashes; however, their results need additional confirmation due to the small magnitudes of World Wide Lightning Location Network (WWLLN) detection efficiencies (DEs), especially at continental locations (see section 2). Their findings are at odds with the findings of Boersma et al. (2005), who estimated continental flashes to be ~1.6 times more productive, based on GOME data. However, they are consistent with earlier findings of more energetic flashes over oceans (Beirle et al., 2014; Chronis et al., 2016).

Satellite observations of LNO_x ($NO + NO_2$ from lightning) combined with ground- or satellite-based lightning flash counts have become increasingly valuable in PE investigations. Satellites directly measure NO_2, which must be converted to NO_x via CTMs. Methods to estimate PE from satellite measurements generally fall into two categories: those using long-term data to constrain CTM simulations so that they match observed NO_x, and those based on retrievals of freshly-produced NO_x, which can be compared to concurrent lightning data. Examples of the former include the model assimilations of Boersma et al. (2005), Martin et al. (2007) and Miyazaki et al. (2014), which yielded NO_x production rates equivalent to mean global PEs of 55 ± 320, 300 ± 100 and 320 ± 70 mol per flash, respectively. More recently Marais et al. (2018) combined 3 years of NO_2 data obtained from the Ozone Monitoring Instrument (OMI) retrieved by cloud slicing (Ziemke et al., 2001; Choi et al., 2008) with lightning measurements from Optical Transient Detector (OTD) and Lightning Imaging Sensor (LIS) and the GEOS-Chem model to obtain a mean PE of 280 ± 80 mol per flash.

Investigations based on freshly produced LNO_x face a number of observational hurdles. Some of these are instrument-related, such as the low spatial resolutions of satellite instruments, which can complicate comparisons with lightning in small-scale convective systems, as well as saturation of instrument pixels over bright convective clouds (L. Lamsal, H. Eskes, private communications). As in assimilation studies, the dominant stratospheric part of the satellite-measured total NO_2 column must be removed from the smaller LNO_2 component. A variety of schemes are used to do this, each yielding different results on sub-synoptic scales (Richter and Burrows, 2002; Wenig et al., 2003; Boersma et al., 2011; Bucsela et al., 2013; Yang, et al., 2014; Beirle et al., 2016). Ambient tropospheric NO_x must also be distinguished from the fresh LNO_x signal. The use of cloudy scenes limits contamination of the lightning signal by NO_x in the lower troposphere with a likely anthropogenic source (Beirle et al., 2010; Pickering et al., 2016; Marais et al., 2018; Allen et al., 2019). High flash-rate restrictions have also been imposed to ensure that lightning NO_x is the predominant component of the satellite signal and that the background contribution is minor (Beirle et al., 2010; Pickering et al., 2016). Subtraction of *a priori* background estimates has also been used (Bucsela et al., 2010; Pickering et al., 2016; Allen et al., 2019). An additional challenge is synchronization of NO_2 data with concurrent lightning measurements. To date, all satellite LNO_x studies have been based on low earth orbit (LEO) instruments, which make, at best, only one NO_2 measurement per day of a given region. Their local time (LT) for overpass is also before the late-afternoon convective peak, as with the Global

Ozone Monitoring Experiment (GOME) (LT=10:30), the Scanning Imaging Absorption Cartography (SCIAMACHY) instrument, (LT=10:00), OMI (LT=13:45) and the Tropospheric Monitoring Instrument (TROPOMI), LT=13:30.

PEs based on fresh LNO_x production have generally yielded smaller PEs than assimilations. Using tropical data from the Tropical Composition, Cloud and Climate Coupling Experiment (TC^4), Bucsela et al. (2010) found a mean PE of 174 ± 219 mol per flash based on OMI NO_2 measurements and lightning data from WWLLN and the Costa Rica Lightning Detection Network (CRLDN). Pickering et al. (2016) estimated a mean PE of 80 ± 45 mol per flash over the Gulf of Mexico, using datasets from OMI and the WWLLN. Over the same region, using GOME data, Beirle et al. (2006) derived a similar value of 90 (range of 32 to 240) mol per flash. However, Beirle et al (2010) obtained a nearly null result in their study of 287 convective events, with no detectable LNO_x enhancement over most storms and overall negligible correlation with flash counts. In a tropical study, Allen et al. (2019) used updated versions of the Pickering et al. (2016) datasets, identical to those of the present study, and estimated a PE of 133 ± 72 mol per flash in the tropics. They also noted a decrease in PE with increasing lightning flash rate.

The present study examines three midlatitude regions (N. America, Europe and East Asia and parts of adjacent waters) over five boreal summers (JJA, 2007 – 2011) to investigate the LNO_x PE. NO_2 observations from OMI are compared with lightning flashes detected by the WWLLN and converted to NO_x using air mas factors based on LNOx and LNO_2 profiles from a chemical-transport model. NO_x retrieved in regions of deep convection without lightning flashes are subtracted as the tropospheric NO_x background. This investigation and the tropical study of

Allen et al. (2019) are the largest scale satellite studies to date (in terms of observed convective events) of the amount of NO_x production from observed flash data. We describe the data in section 2, methods in section 3, and results in section 4. Results and discussion, including uncertainty estimates are presented in sections 4 and 5 respectively, and section 6 is a summary.

2. Data description

2.1 OMI

The Dutch-Finnish OMI spectrometer is one of four instruments on NASA's Aura satellite, launched July 15, 2004 (Schoeberl et al., 2006; Levelt et al., 2006, 2018). The satellite is in a sun-synchronous orbit with equator and midlatitude crossing times of 13:45 and ~13:30 local time (LT), respectively. OMI operates in push-broom configuration with a swath spanning 2600 km. In normal mode there are 60 pixels across the swath, and the field of view (FOV) of nadir pixels is 13 x 24 km^2. There are ~1600 swaths per orbit and ~15 orbits per day. Midlatitude LTs across a swath can differ from nadir by as much as ±1 hour, and there is significant overlap between adjacent orbits. However, averaging of data in the present study minimizes the effects of LT variation. Beginning in 2007, OMI pixels were affected by the row anomaly (RA), first described by Dobber et al. (2008). The RA reduced valid data across each swath by ~3 to ~30 pixels between 2009 and 2011, and doubled the time required for global coverage from 1-2 days. Bad-pixel flagging and CCD dark current also grew by a factor of ~2 during the 2007 – 2011 period, and signal-to-noise ratio (SNR) has decreased (Shenkeveld, et al., 2017).

NO_2 slant columns densities (SCDs) used in this study are obtained from the v3 NASA OMI NO_2 standard data product (Marchenko et al., 2015; Krotkov et al. 2017). Relative to SCDs in the previous v2.1 product (Boersma et al., 2011; Bucsela et al., 2013), the v3 SCDs are 10 – 40% smaller. The v3 algorithm employs an iterative spectral fitting routine in the 402 – 464 nm range that corrects errors in wavelength registration and separately fits a Ring spectrum and absorption cross sections for NO_2, H_2O and $C_2H_2O_2$. Data quality at these wavelengths has been relatively stable over the instrument's lifetime. Radiometric degradation, stray light interference and wavelength calibration errors have remained below 3%, 0.5% and 0.002 nm, respectively (Dobber et al., 2008; Marchenko and DeLand, 2014; Schenkeveld et al., 2017). However, NO_2 SCD measurements between 2005 and 2015 over the central Pacific showed an increase in standard deviation from 0.8×10^{15} to 1.0×10^{15} cm^{-2} (Krotkov et al., 2017).

NO_2 SCDs are combined with level-2 NO_2 stratospheric vertical column densities (VCDs) and stratospheric air mass factors (AMFs), also from the v3 product. AMFs are based on *a priori* cloud and terrain inputs as well as chemical-transport and radiative-transfer model output. Cloud optical centroid pressure (OCP) and cloud radiance fraction (CRF) are obtained from the OMI O_2-O_2 algorithm, where OCP is the effective cloud-top pressure visible from OMI (Acaretta et al., 2004; Sneep et al., 2008; Stammes et al., 2008; Vasilkov et al., 2009). Terrain pressures and reflectivities are obtained, respectively, from a digital elevation model and OMI clear-sky measurements (Kleipool et al., 2008). The Global Modeling Initiative (GMI) chemistry-transport model (section 2.3) computes monthly NO_2 profile shapes and tropopause pressures for the AMFs. Atmospheric scattering weights are calculated by TOMRAD (Davé, 1965). The AMFs are also used in the stratosphere-troposphere separation algorithm (STS) (Bucsela et al., 2013) to derive the stratospheric VCDs from the total SCDs.

2.2 WWLLN

The World Wide Lightning Location Network is a continuously operating ground-based global array of VLF radio wave sensors that detect very low frequency (VLF) sferics from lightning (Dowden et al., 2002; Lay et al., 2005; Virts et al., 2013). The number of active sensors grew from 11 at initial global deployment in 2003 to ~30 in 2007, to ~60 in early 2012 (Hutchins et al., 2012). The increase between 2003 and 2007, alone, led to a growth in the number of lightning detections by ~165%. Globally, detection efficiencies (DEs) were estimated by Rodger et al. (2006, 2009) and Abarca et al. (2010) to be ~10% based on comparisons with regional networks, and this value has increased in recent years. Detection range is ~10,000 km, allowing reasonable coverage with a sparse array (Lay et al., 2005; Rodger et al., 2009). Spatial and temporal accuracies are ~5 km and < 10 μs, respectively (Abarca et al., 2010). Sensitivities are higher for CG than IC flashes (Rodger et al., 2009; Rudlosky and Shea, 2013), although we do not distinguish between the two in the present study.

WWLLN detections are calibrated against OTD/LIS climatological data (Cecil et al., 2014). Comparisons are limited to the latitude ranges of the instruments, which are $\pm 35^o$ for LIS and $\pm 70^o$ for the older OTD. Details of the calibration and calculation of WWLLN DEs are described by Pickering et al. (2016) and updated WWLLN processing is given by Allen et al. (2019). In brief, monthly WWLLN flash counts from 2007 to 2014 are smoothed temporally and spatially and compared to an OTD/LIS climatology (Boccippio et al., 2000, 2002; Cecil et al., 2014) to obtain monthly DE values on a 2° longitude × 2.5° latitude grid. These are re-gridded on a 1° longitude × 1° latitude grid and a diel adjustment is applied. In the present study, the DEs are modified *a posteriori* so that global WWLLN hourly counts are consistent with the OTD/LIS Low Resolution Annual Diurnal Climatology, which has a 2-hour temporal resolution (Cecil et al., 2014). The diel variation of WWLLN counts are also examined with respect to time-resolved data from the North Alabama Lightning Mapping Array (NALMA) (Koshak et al., 2004).

Figure 1 shows WWLLN sensor locations and northern hemisphere detection efficiencies. As described below, the domain of this study includes (1) eastern North America and the western Atlantic, (2) Europe and (3) East Asia and the western Pacific, where area-weighted DEs in 2007 (2011) were 3.6 (10.6), 2.3 (4.5), and 2.7 (8.0) percent, respectively. These values correspond to an average ~3 – 8% increase over 5 years in the probability that WWLLN detects a given flash. Since most flashes occur over land, where DEs are smaller (see Figure 1), the actual fraction of flashes detected by WWLLN is 10 – 50% less than the area-weighted DE. The small magnitude and high spatial and temporal variability of the DE make the WWLLN flash counts a major source of uncertainty in the present results.

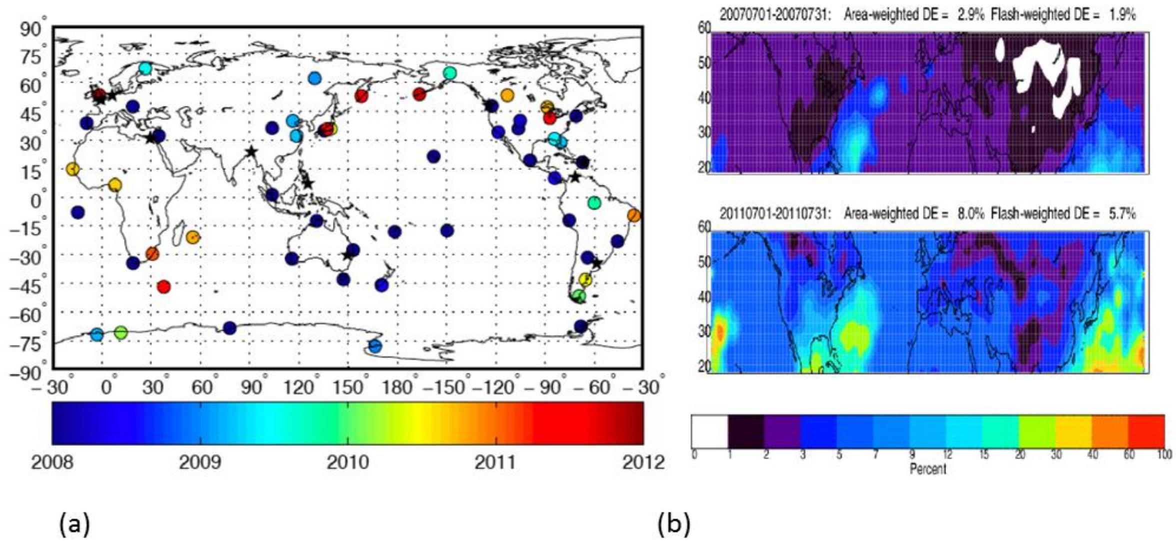

Figure 1: (a) WWLLN sites, color coded by first date of operation. Dark blue circles indicate stations in operation 2007 or earlier (b) WWLLN detection efficiencies between 1230 and 1330 LT for July 2007 and July 2011, calibrated against OTD/LIS climatology. The mean area and flash-weighted DE for each period are shown in the figure.

2.3 GMI

NASA's GMI model (Ziemke et al., 2006; Duncan et al., 2007; Strahan et al., 2007, 2013; Allen et al., 2010) is used in both the OMI standard NO_2 product and here to estimate shapes of LNO_2 and LNO_x vertical profiles for AMF calculations. GMI is a chemical transport model that also accounts for radiation, deposition and aerosol mass concentrations, but does not include the effects of nitrate aerosols which might affect total NO_x columns in heavily polluted areas. The GMI simulations for this study were driven by meteorological fields from GEOS-5 MERRA (Modern Era Retrospective analysis for Research and Applications) (Rienecker et al.., 2011). Year-specific monthly mean GMI output was computed for 2007 – 2011 using Emission Database for Global Atmospheric Research (EDGAR) 2000 fossil fuel data and biomass burning emissions inventories (van der Werf et al., 2010) with annual scaling factors from the Goddard Earth Observing System-Chemical Transport Model (GEOS-Chem) (van Donkelaar et al., 2008). In this study, we compute LNO_2 and LNO_x profiles as the difference between model output with and without a lightning source. The lightning contribution is based on Allen et al. (2010) and assumes a PE of 500 mol per flash poleward of ± 26° and 250 mol per flash equatorward of ± 26°. AMFs are relatively insensitive to the magnitude of the *a priori* PE, but do depend significantly on profile shapes and NO_x partitioning.

2.4 Data domain

The domain for this study was selected based on the quality of available OMI and WWLLN data. Increases in noise and the effects of the row anomaly significantly compromised OMI data from 2009 onwards. However, increasing WWLLN DEs reduced uncertainties in the WWLLN flash counts during the same period. The five summers of 2007 - 2011 were chosen as a compromise between the years of highest OMI and WWLLN data quality. Measurements during this period were taken in three midlatitude regions having high climatological lightning frequency. The regions are (1) the eastern and central United States and southern Canada along with adjacent parts of the western Atlantic, Gulf of Mexico and Caribbean between longitudes -115^{o} and -55^{o} and latitudes 20^{o} to 60^{o}, (2) Europe and the Mediterranean, between longitudes -10^{o} and -60^{o} and latitudes 30^{o} to 60^{o}, and (3) East Asia and the western Pacific between longitudes 90^{o} and 150^{o} and latitudes 20^{o} to 60^{o}. Further data selection criteria are in section 3.

3. Method

Here we describe retrieval of LNO_x amounts from the level-2 OMI NO_2 data. Vertical-column tropospheric NO_x over deep convective grid boxes (V_{LNOx}*) is derived from OMI pixel data by Equation 1,

$$V_{\mathrm{LNOx}}^* = (S - V_{\mathrm{stratZonal}}\, A_{\mathrm{strat}}) \,/\, A_{\mathrm{LNOx}}, \qquad (1)$$

where S is the total SCD from the OMI NO_2 spectral fit version 3.0 algorithm (Marchenko et al., 2015). A_{strat} is the stratospheric air mass factor, which depends on viewing geometry. A_{LNOx} is the air mass factor that converts the tropospheric NO_2 slant column to the NO_x vertical column, denoted here as V_{LNOx}^* (see Pickering et al., 2016; Allen et al., 2019). The asterisk indicates that the vertical column includes contributions from non-lightning NO_x sources and non-recent lightning, i.e., a background correction has not been made. $V_{\mathrm{stratZonal}}$ is the zonally averaged v3 stratospheric VCD (V_{strat}) (Bucsela et al., 2013; Krotkov et al., 2017). It is obtained by smoothing V_{strat} in pixels with CRF > 0.97 and OCP < 500 hPa, using a $\pm 180^{o}$ longitude and $\pm 3^{o}$ latitude running boxcar. Zonal smoothing eliminates longitudinal variations in stratospheric NO_2 concentration, tropopause height and the *a priori* troposphere used in the STS algorithm. The smoothing is needed because the STS algorithm can erroneously assign small amounts of tropospheric NO_2 to the stratosphere (Bucsela et al., 2013; Beirle et al., 2016; Allen et al., 2019). We multiply the smoothed stratospheric VCD by the stratospheric AMF and subtract from the total SCD to obtain the tropospheric NO_2 SCD, i.e., the term in parentheses in Equation 1.

The tropospheric SCD is divided by an air mass factor, A_{LNOx}, computed from model GMI NO_2 and NO_x profiles and TOMRAD (Davé, 1965) scattering weights. The profiles were created using the difference between model runs with and without a lightning source of NO. Following Pickering et al. (2016), the profile at a given location is chosen from the day with the 3rd largest LNO_x column during a given month and year and is considered representative of moderate-to-active convective environments. Midlatitude profile examples for June 2007 are shown in Figure

2. Conceptually, A_{LNOx} is the ratio of the modeled tropospheric LNO_2 SCD to the modeled LNO_x* VCD from tropopause to ground. Retrieved V_{LNOx}* therefore includes LNO_x* below the OCP that cannot be directly observed by OMI. For the domain of this study, the mean OMI OCP is 483 hPa with a standard deviation of ~100 hPa. The corresponding GMI fraction of the LNO_x column below the OCP is ~10 – 30%. This range is consistent with profiles from the cloud-resolved simulations of Ott et al. (2010) from the CRYSTAL-FACE campaign.

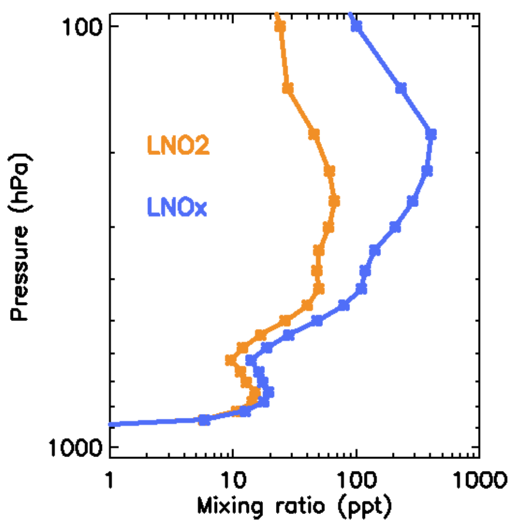

Figure 2: 2007 June profiles of LNO_2 and LNO_x from GMI for longitude -85 E, latitude 40 N. Profiles are the difference between NO_2 (NO_x) from simulations without lightning and NO_2 (NO_x) from simulations with a lightning source of NO.

Only pixels with CRF > 0.97 and OCP < 500 hPa are used in the analysis. These restrictions favor data from the bright, opaque clouds associated with deep convection (Pickering et al., 2016) and minimize contamination by low and mid-level NO_2, especially over low-level stratus clouds, which enhance visibility of ambient NO_2 immediately above them (Martin et al., 2002).

LNO_x^* vertical columns are binned in the 1° longitude × 1° latitude grid boxes used for the WWLLN flashes, with a minimum of 3 OMI pixels per box. The number of LNO_x* molecules in each box is obtained by multiplying the average of the vertical columns from the pixels by grid box area. This scheme was chosen over pixel-area weighting (e.g. Nault et al., 2017), which imparts greater weight to pixels at swath edges, where adjacent orbits overlap and local times can differ from local time at nadir (13:30 LT) by as much as 1 hour. Without this weighting, edge pixels contribute less than nadir pixels because they are sparser. We count WWLLN flashes in a 1-hour window prior to the 13:30 LT OMI overpass. This window minimizes advection of LNO_x out of boxes before the OMI measurement. The choice of 1 hour is based on mean midlatitude GEOS-5 MERRA upper tropospheric (UT) wind speeds, which are estimated in the range 11 to 21 m/sec. It is shorter than the 3-hour window used by Pickering et al. (2016) in their Gulf of Mexico study, where summertime UT wind speeds are 6 to 11 m/s.

A tropospheric NO_x background is subtracted from the LNO_x^* in each grid box to remove ambient NO_x not generated within the 1-hour flash window. The background is a weighted temporal average of boxes at each geographic location having 0 – 1 flashes during the window. Background boxes are subject to the same OCP and CRF restrictions as boxes with lightning and are weighted according to the number of OMI pixels contributing to each. The gridded background is smoothed with a $5^o \times 5^o$ boxcar to lessen noise and fill in gaps. Subtraction of the 2-D background array from the 3-D array (longitude, latitude, day) of LNO_x* yields an array of "flashing boxes" containing freshly-produced LNO_x.

LNO_x was corrected for convectively lofted pollution and chemical decay. The amount of lofted pollution is assumed to be proportional to LNO_x, as both are assumed to scale with convective updraft strength. Therefore, pollution is considered a fraction of the LNO_x signal, rather than a component of the mean background, which consists of boxes without active lightning. The magnitude is derived from DeCaria et al. (2000; 2005), who examined a midlatitude storm NNE of Denver near the Wyoming border on a day with boundary layer (BL) flow from the east. They estimated pollution to comprise < ~20% of total anvil-level NO_x. We choose a slightly lower 15% pollution correction to account for the mix of rural and urban regions in the data domain. The estimate of chemical decay is based on the 3-hour LNO_x lifetime of Nault et al. (2017), which is based on measurements in near-field convective outflow. With this value, the average decay over a 1-hour period is ~15%, and we adjust measured LNO_x upward accordingly. This adjustment approximately cancels the lofted-BL NO_x correction.

4. Results

4.1 Geographic distribution

Maps of OMI and WWLLN data are shown in Figure 3. The red boxes outline the 3 areas of study – eastern North America, Europe and East Asia. The fields shown are 15-month temporal means of daily observations of $V_{\mathrm{init}} - V_{\mathrm{StratZonal}}$ (ΔV_{NO2}), LNO_x*, LNO_x and lightning. V_{init} is the "initial" vertical column retrieved from OMI, defined as S / A_{strat}, or the ratio of the total OMI NO_2 slant column to the (approximately geometrical) stratospheric AMF. As such, it depends only on the OMI spectral fit with no further geophysical assumptions. In the figure, the fields have been smoothed with a 3° longitude × 3° latitude boxcar for clarity. Qualitatively Figure 3 shows that the three regions of study contain higher ΔV_{NO2}, LNO_x*, LNO_x and lightning relative to other northern midlatitude areas. Spatial correlations of LNO_x* with lightning are highest in China and the southeastern United States. These regions also have the highest mean flash rates.

Pearson's correlation coefficients, *r*, between LNO_x* and lightning are 0.22, 0.12, 0.25 and 0.22 for North America, Europe, East Asia and the combined region, respectively. Correlations between LNO_x and lightning are weaker, in part due to noise in the subtracted background, but can be seen qualitatively on scales of ~2000 km. The *r* values for LNO_x are 0.16, 0.15, 0.21 and 0.18 for North America, Europe, East Asia and their sum, respectively. Regions with low WWLLN detection efficiencies may be misclassified as background, lessening the contrast between flashing and non-flashing boxes and reducing the LNO_x signal. For example, the LNO_x* enhancement over NW India and Pakistan is weak in the LNO_x field. Lightning climatologies from OTD/LIS do show enhanced lightning in this region (Cecil et al., 2014), but detected flashes are few during the time immediately preceding OMI. The disparity may indicate poor WWLLN coverage with incorrect DE estimates, an inaccurate diel distribution of flashes, or ambient LNO_x* from earlier convection. Differences in the LNO_x* and LNO_x fields in the southeastern U.S. that are less prominent in the LNO_x field may also result from lightning before the 1-hour flash window, including recirculation around the Bermuda High (Cooper et al., 2006, 2007).

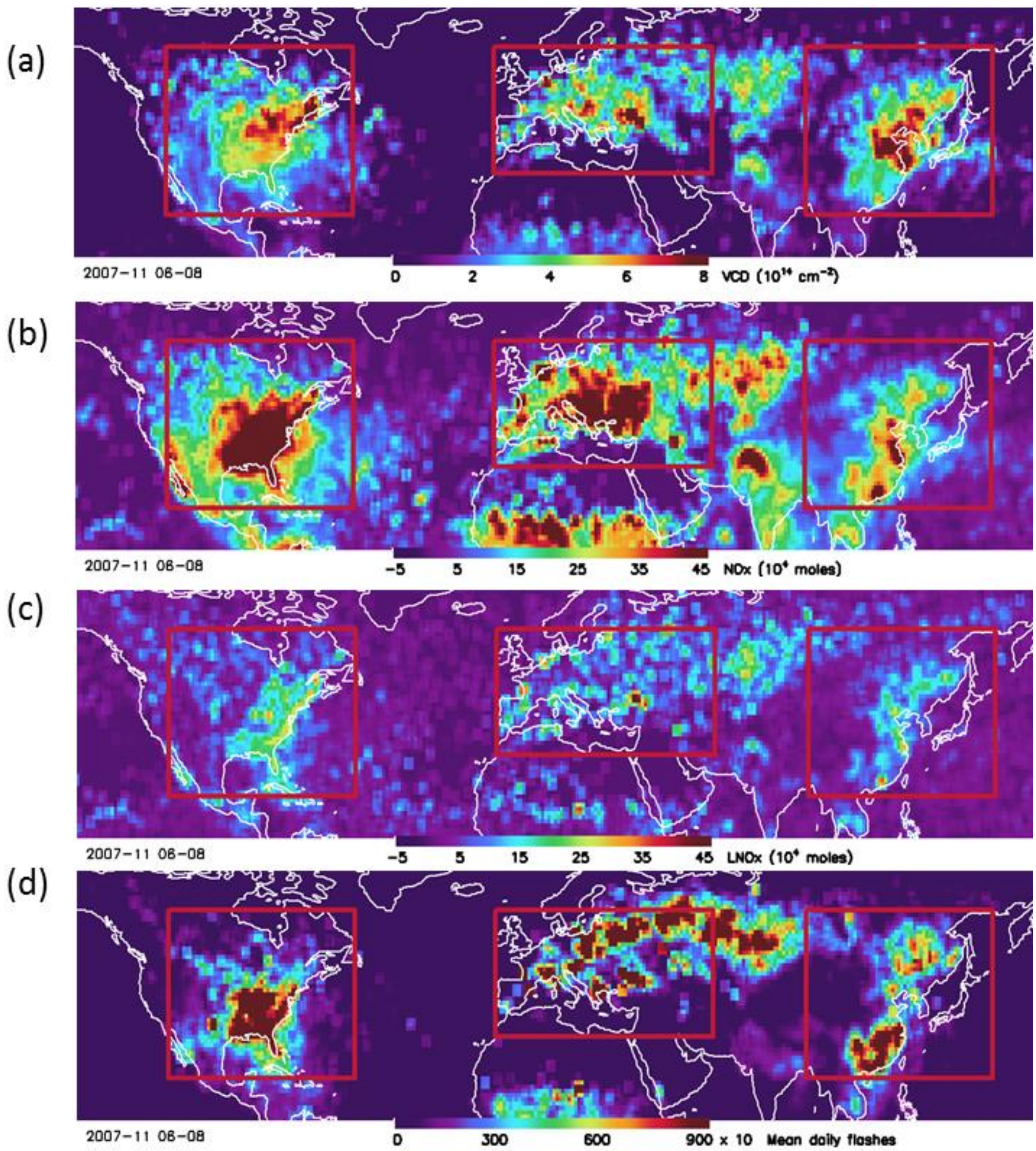

Figure 3: Mean daily data for JJA 2007 – 2011 per 1° longitude × 1° latitude box, averaged over flashing boxes. (a) ΔV_{NO2} (10^{14} cm^{-2}), (b) LNO_x* (1×10^6 moles), (c) LNO_x (1×10^6 moles), (d) mean daily WWLLN flash counts in flashing boxes (× 10). The red boxes outline the 3 geographic regions (North America, Europe and East Asia) examined in this study.

4.2 Mean production efficiency

The 15-month LNO_x and 1-hour flashes were summed over all grid boxes in the data domain to estimate an average PE. Mean LNO_x is 130 kmol per flashing box, which is 45% of mean LNO_x*. On average, the same flashing boxes contain 740 WWLLN flashes. We compute the ratio of total LNO_x to total flashes and obtain an average PE of 180 ± 100 moles LNO_x per flash. Bias and error estimates are discussed in section 5. If this PE value is representative of all flashes globally, combining it with the estimated mean global flash rate (Cecil et al., 2014) would yield an annual global LNO_x budget of 3.5 ± 2.0 Tg N/yr.

4.3 Data correlations

In Figure 4, ΔV_{NO2} and LNO_x from individual flashing boxes are plotted against 1-hour kflashes. The points represent the ~32,000 flashing boxes in the data set. Approximately 39% of the these have negative LNO_x values due, in part, to overestimation of the tropospheric background at those locations. ΔV_{NO2} also contains negative values, indicating some overestimation of stratospheric NO_2. Data at higher flash rates are relatively sparse, with less than 10% of flashing boxes containing over 2 kflashes per hour and ~1% having rates exceeding 6 kflashes per hour. Because of these issues, any relationship between the OMI data and lightning is difficult to discern in the figures. Correlation coefficients are r = 0.20 for ΔV_{NO2} and 0.18 for LNO_x.

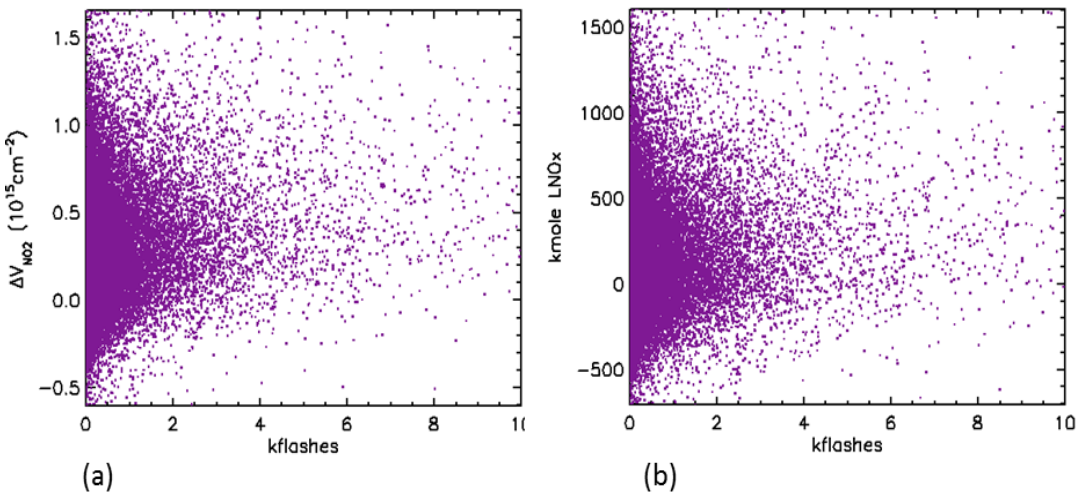

Figure 4: Scatterplots of (a) ΔV_{NO2}, and (b) LNO_x vs 1-hour flashes for all flashing boxes.

Although the correlations are not large, they are significant. This can be seen by comparing correlations between WWLLN flashes in a given box with OMI-derived LNO_x in other boxes. The plots show r values when flash counts are compared with LNO_x in surrounding boxes on the same and different days. In Figure 5b, the r = 0.18 appears in the central box and represents the value for the LNO_x correlation with lightning in the same boxes on the same days. The correlations in surrounding boxes are lower and may be due to advection and/or lightning occurring before the 1-hour integration period. The slight enhancement northeast (to the upper right) of the central box is consistent with the typical southwesterly flow environment for northern midlatitude convection (e.g. Markowski and Richardson, 2011). Figures 5a and 5c also illustrate spatial correlations but compare LNO_x on a given day with 1-hour flashes from the preceding and following days, respectively. In the central boxes, LNO_x shows minimal correlation with lightning from the previous day (maximum value of r = 0.08 in the central box) and ~none with lightning on the next day (r = 0.04 in the central box). Together these results are strong evidence that a sizeable portion of the LNO_x in each grid box is produced by lightning flashes in the same box during the hour before OMI overpass.

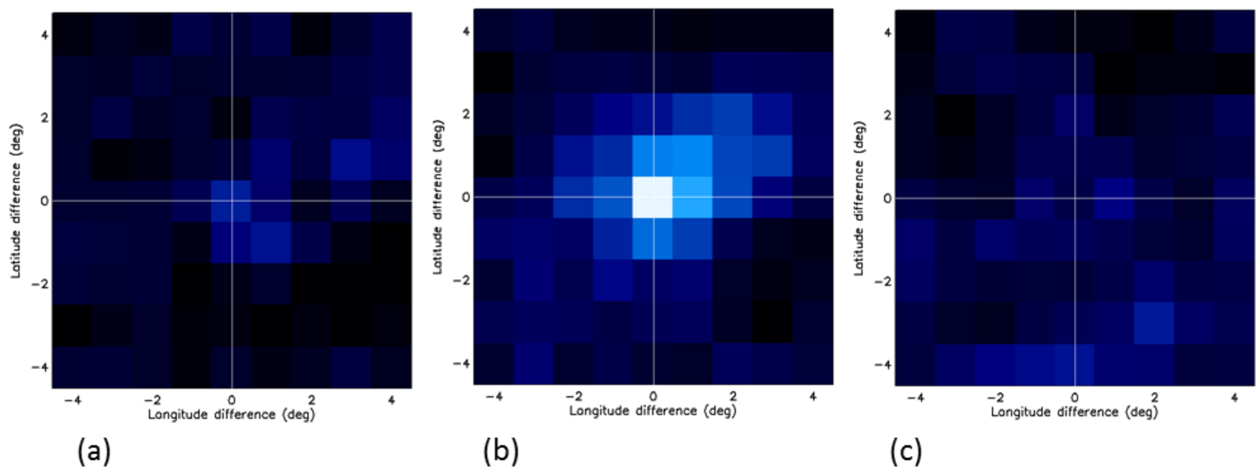

Figure 5: Spatial correlations between LNO_x and 1-hour lightning flashes. The 3 panels show correlations of LNO_x with (b) lightning on the same day, (a) lightning on the preceding day and (c) lightning on the following day. The dimensions of the boxes correspond to the 1° × 1° grid cells. North is up and east is to the right. Color scale ranges linearly from r = 0.0 = black to r = 0.18 = white.

A relationship between the OMI and WWLLN data becomes clearer when the lightning-NO_x metrics V_{init}, ΔV_{NO2}, LNO_x* and LNO_x are binned by flash rate, as shown in Figures 6a, 6b, 6c and 6d, respectively, using three OCP thresholds. The fields in 6a–d represent successively greater amounts of processing applied to the OMI data. Specifically, V_{init} depends only on OMI slant columns (and a geometrical AMF), ΔV_{NO2} assumes a stratospheric estimate, LNO_x* adds the assumption of a model-based AMF, and LNO_x includes the additional tropospheric background estimate. All fields exhibit qualitatively similar behavior, showing a non-linear dependence on flash rate, with the slopes of the curves implying a decrease in production efficiency as flash rate increases. The curves in 6a – 6d are also somewhat more linear for OCP < 400 hPa than for larger OCP thresholds, resulting in higher LNO_x* and LNO_x (6c and 6d) at the highest flash rates (see section 4.5). However, V_{init} and ΔV_{NO2} (6a and 6b) are both uniformly lower at all flash rates for OCP < 400 hPa, due to neglect of LNO_2 in those fields below the OCP altitude. We quantify these effects below and discuss geophysical bases for the nonlinearity in section 5.

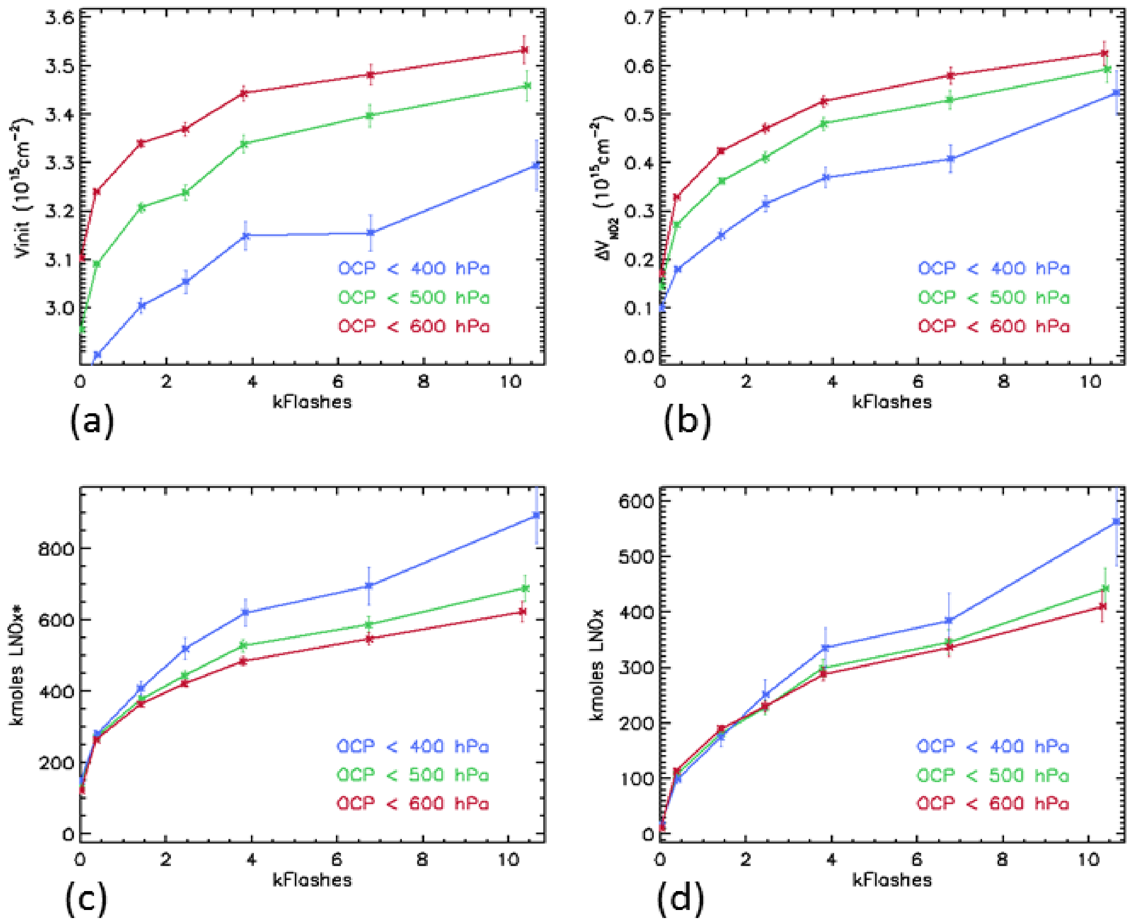

Figure 6: Binned values of (a) V_{init} (10^{15} molec cm^{-2}), (b) ΔV_{NO2} (10^{15} molec cm^{-2}), (c) LNO_x* (moles), and (d) LNO_x (moles) as functions of 1-hour flashes. OMI data are binned in seven WWLLN flash-rate bins, with CRF > 0.97 and minimum OCPs of 400, 500 and 600 hPa.

4.4 Quantitative dependence of PE on flash rate

In Figure 7, LNO_x are averaged in 500-flash-per-hour bins between 0 to 10,000 flashes per hour, with each bin containing at least 3 flashing boxes. The linear correlation coefficient for the binned data is r = 0.87. Two weighed fits were performed: an ordinary least squares linear fit (blue) and a power function fit (red) given by

$$y = a + b\,x \qquad (2)$$

$$y = \alpha\, x^{\beta} \qquad (3)$$

respectively, where x is kflashes and y is kmoles LNO_x. Weights are inverse standard errors of the mean, shown as error bars. The LNO_x PEs are the derivatives of Equations (2) and (3). For the linear fit we find a = 79 ± 29 kmole and b = 64 ± 10 mol per flash, where b is the regression-based PE, assuming a linear relationship between flashes and LNO_x. The power law coefficient is α = 8.0 ± 0.8 kmole, with exponent β = 0.45 ± 0.01. Fits to the un-binned LNO_x data yield a = 94 kmole, b = 45 mol per flash, α = 10.3 kmole and β = 0.42, with negligible standard errors. While binning clarifies the relationship between LNO_x and flashes, the comparable fitted values suggest results do not depend strongly on binning scheme (see also section 4.5). Reduced chi squares (χ^2_r) for the linear and power-function fits to the binned data are 10.1 and 1.5, respectively. The comparison shows the power function to be a much better fit than a straight line. In Figure 7a, the data are plotted with linear scaling on the axes, while Figure 7b is a log-log plot. The slope of the orange line in 7b corresponds to a direct proportion (constant PE) between moles LNO_x and flashes, while the horizontal green line represents no relation between the two (vertical placement of the orange and green lines is arbitrary). The power function with β ~ 0.4 lies between the two. The slope of power function fit corresponds to a PE that decreases by over an order of magnitude, from 290 to 20 mol per flash for flash rates between 100 and 10,000 per hour. The average PE of 180 mol per flash derived from all flashes and LNO_x over the entire data domain is intermediate between these values.

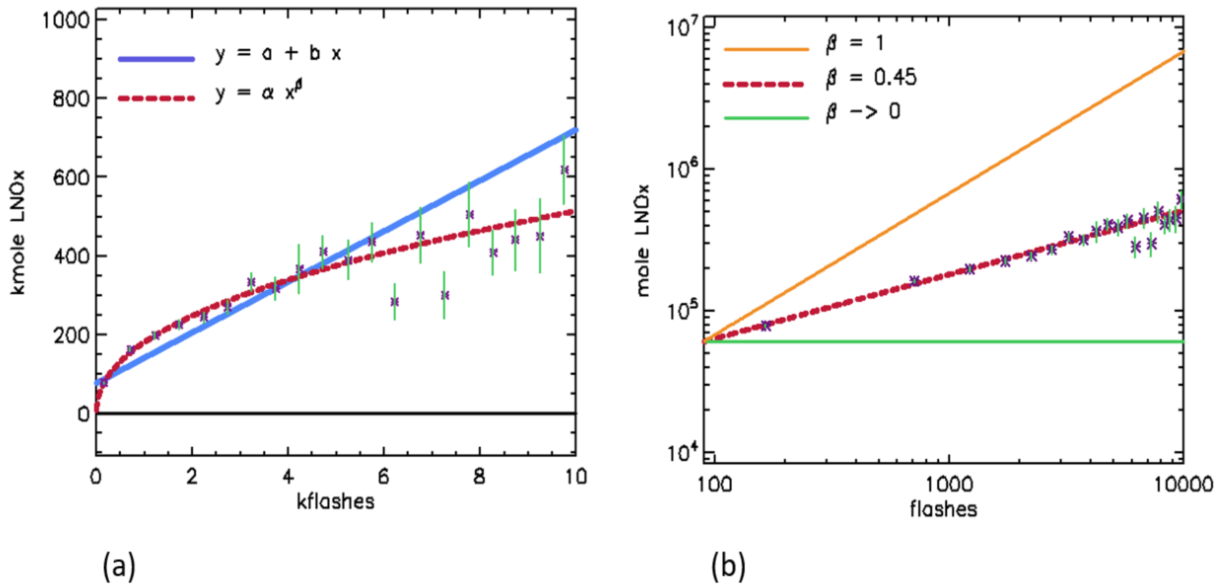

Figure 7: LNO_x (1×10^3 moles) vs 1-hour flash rates (1×10^3 flashes) using data binned by flash count. (a) Linear axis scaling and (b) Log-log axes. Blue and dashed-red lines are linear and power-function fits to the data, respectively, with the PE as the slope of each. Slopes of the orange and green lines indicate a direct proportion between LNO_x and flashes and no relationship, respectively (vertical placements are arbitrary).

Figure 8 shows that the flash-rate dependences for the three individual midlatitude regions are similar to that of the combined region. The smaller datasets in North America and Europe yield *r* values of 0.59 and 0.42, respectively, which are less than found in the combined region. However, the value of *r* for East Asia is 0.86, approximately the same as the combined value. The reduced chi-squares for each of the three regions all support a non-linear relationship between flashes and the LNO_x produced. Average PEs obtained by summation in each region are comparable, with values for North America, Europe and East Asia of 200, 150 and 160 mol per flash, respectively. Results are summarized in Table 1.

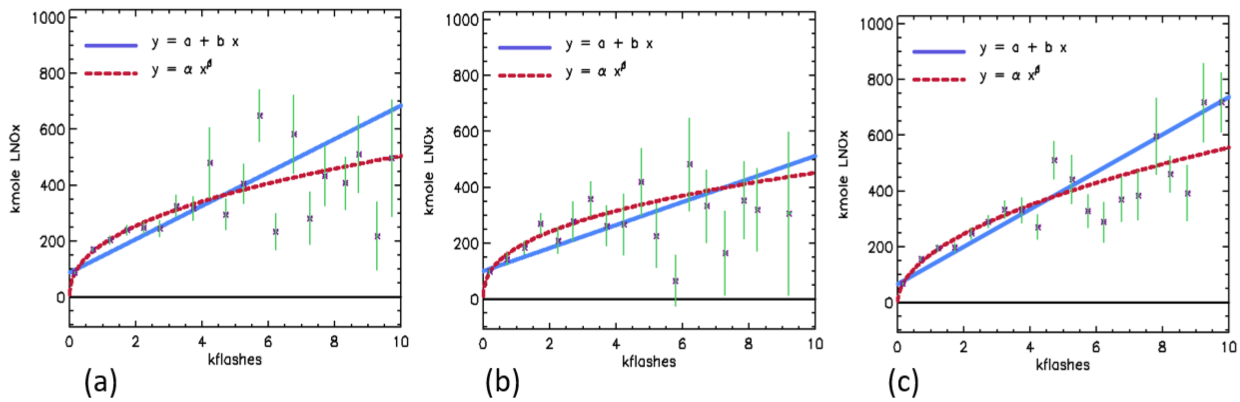

Figure 8: LNO_x (1×10^3 moles) vs 1-hour flash rates (1×10^3) using data binned by flash count for (a) North America, (b) Europe and (c) East Asia. Blue and red lines are linear and power-function fits to the data, respectively. Values for b and β here and in Fig. 7 are given in Table 1.

Table 1

Average PE and regression analysis of binned data from the 3 geographic regions separately and combined. Statistics are computed with flashes averaged in 20 bins of 0.5 kflashes/hour.

Region	r	b (mol per flash)	β	χ^2_r (linear)	χ^2_r (power)	PE_{avg} (mol per flash)
N. Am.	0.59	60	0.42	5.79	1.84	200 ± 110
Europe	0.42	41	0.39	2.04	1.40	150 ± 90
E. Asia	0.86	67	0.51	5.77	1.78	160 ± 100
Combined	0.87	64	0.45	10.1	1.49	180 ± 100

4.5 Dependence on OCP

Vertical profiles of mean flash rate and mean LNO_x as a function of OCP are shown in Figure 9. Flash and LNO_x values for flashing boxes have been averaged in 30 hPa-wide bins. The average flash rate increases with decreasing OCP (Figure 9a), indicating more frequent flashes in deeper convection. This result is in qualitative agreement with the findings of Williams et al. (1985) and Price and Rind (1992), who describe a power-law dependence on altitude, with exponents of ~5 and 1.7 for continental and marine regions, respectively. However, the WWLLN flash rates here have significantly weaker altitude dependence, corresponding to an exponent of 0.87 ± 0.04, as indicated by the dashed line. The 5th power dependence is theoretical and based on IR cloud-top heights rather than OCP-derived altitudes as here. Significant averaging is used in the flash-count processing, which could also affect the apparent altitude dependence. Figure 9b shows average LNO_x as a function of OCP. LNO_x increases with altitude at large OCPs but decreases and becomes more variable above the 450 hPa level. The cause of the decrease could be related to a bias in the model profiles below the OCP, although a somewhat weaker altitude dependence of LNO_x is plausible at higher altitudes, where increases in LNO_x due to more flashes may be countered by decreases in PE. This behavior contrasts with the finding of Boersma et al. (2005) that LNO_2 increases with the 5th power of altitude, a result similar to the continental flash-rate dependence of Price and Rind (1992).

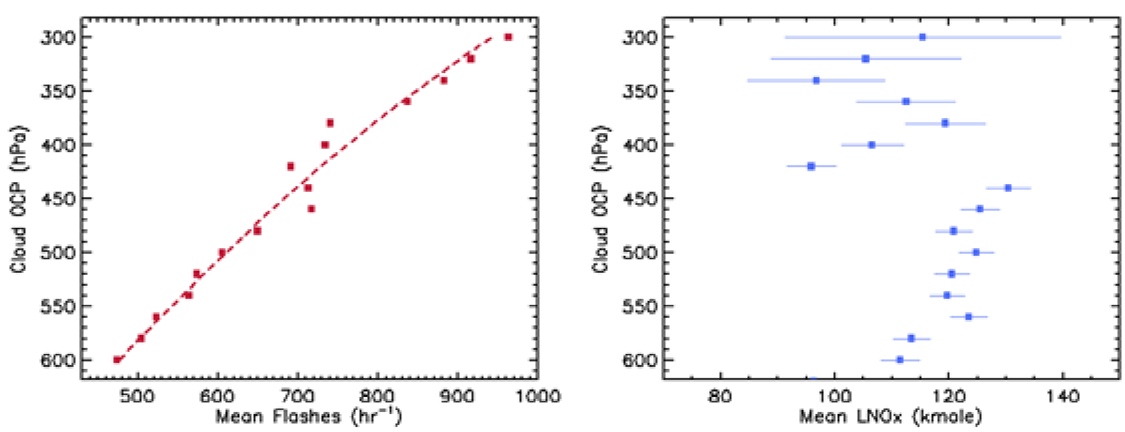

(a) (b)

Figure 9: Profiles of (a) hourly flash rate and (b) LNO_x (1×10^3 moles) vs OMI OCP (hPa) (the y-axis). Data have been averaged in 30 hPa-wide bins. The dashed line in (a) is a power-law fit to the lightning data.

As noted in section 4.3, Figure 6 shows that the flash-rate dependence varies with OCP range. The fields V_{init}, ΔV_{NO2} LNO_x* and LNO_x exhibit a slightly more linear relationship with flash rate at smaller OCPs (higher cloud tops). Exponents, β, for a power-law fit to LNO_x vs flash, binned as in Figures 7 and 8, are 0.55, 0.45 and 0.40 at OCP thresholds of 400, 500 and 600 hPa, respectively. Fitting statistics are shown in Figure 10 as a function of the number of bins in the 0 to 10,000 flash-per-hour range. The correlation coefficient, r, decreases from roughly 0.9 to 0.5 at all OCPs (with a small overall decrease towards smaller OCPs) as the number of bins increases from 20 to 200, due to increased scatter. With OCP thresholds of 500 and 600 hPa, reduced chi-squares for the linear fits decrease from approximately 12 to 3.5 and >12 to 4.5, respectively, while those for the power-function fits are relatively constant at ~1.5. For an OCP threshold of 400 hPa, the respective reduced chi-squares for the linear and power-function fits have ~constant values of 3.5 and 2.5. At that threshold, the smaller disparities between linear and power function fits as well as the weaker dependence of the linear fit on number of bins result from both poorer statistics (due to sparser data above the 400-hPa level) and β values closer to unity than for larger OCP thresholds. Qualitatively, it was found that this OCP dependence does not depend significantly on the form of the OCP restrictions (e.g. whether OCP thresholds or narrow ranges of OCP values are specified), the model-estimated fraction of LNO_x below OCP (implicit in A_{LNOx}), or whether a background is subtracted. Furthermore, there is no known dependence of WWLLN DE on cloud-top height. The effects could conceivably result from variations in flash properties, including duration, extent and radiance, for high- and low-topped convection, but further exploration is needed to draw any conclusions regarding geophysical causes. The role of flash extent is examined in section 5.

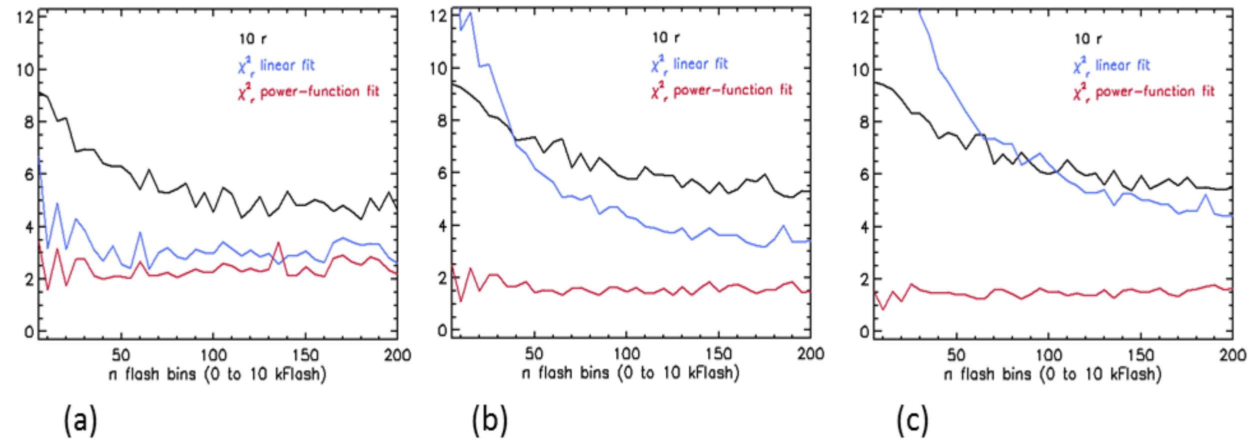

Figure 10: Fitting statistics for data with flash counts between 0 and 10,000 flashes per hour, binned into *n* flash bins (*x*-axis). On the *y*-axis (unitless) are plotted correlation coefficient *r* (×10) and reduced chi-squares for fits (χ^2_r) of LNO_x to 1-hour flash counts at OCP thresholds of (a) 400 hPa, (b) 500 hPa and (c) 600 hPa.

5. Discussion

5.1 Flash-rate dependent production

The present results are the first satellite-based study to suggest that LNO_x production follows a power function with exponent $\beta < 1$. This relationship appears robust at rates above ~100 flashes per hour per grid box but must be modified near a zero-flash rate to avoid an infinite PE. The mean PE is a weighted average of PEs at specific flash rates with weights proportional to the number of flashes at each rate. For a unit flash integration period, let *N* be the total number of flashing boxes. Also let *x* be the flash rate per box, *f*(*x*) be the PE and *p*(*x*) *dx* be the probability of a flash rate between *x* and *x* + *dx*. Integrating over flash rate, the total number of flashes is

$$\phi = N \int x\, p(x)\, dx\,, \tag{4}$$

The corresponding number of moles LNO_x produced is

$$\mu = N \int x \; f(x) \; p(x) \, dx \qquad (5)$$

and the weighted production efficiency is PE = μ / ϕ. Figure 11a, 11b and 11c are histograms of $p(x)$, $x\,p(x)$, and $f(x)$. All three quantities decrease with flash rate, and 11b indicates that total flash count is dominated by storms with the lowest flash rates. Flash rates in the 32,000 flashing boxes range from 1 to 45,000 flashes per hour. Approximately 90% of boxes have rates less than 2000 per hour and these account for 50% of all flashes.

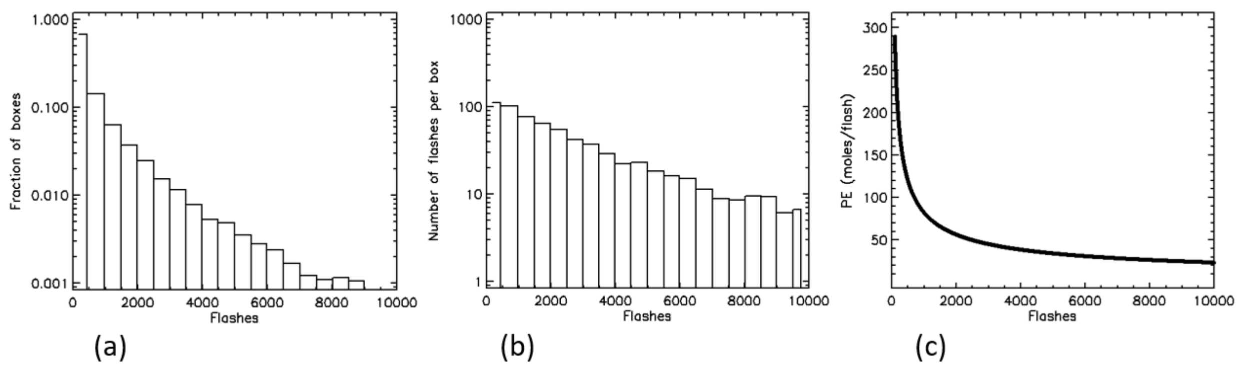

Figure 11: Histograms of (a) $p(x)$ = fraction of flashing boxes in each flash bin, (b) $x\,p(x)$ = number of flashes in each flash bin, (c) $f(x)$ = production efficiency as a function of binned flash rate.

The smaller PE at high flash rates may explain difficulties in detecting significant LNO_x in some studies. Pickering et al. (2016) imposed a minimum threshold of 1000 flashes per hour in $1^o \times 1^o$ grid boxes and obtained a relatively low PE of 80 mol per flash. The 287 cases examined by Beirle et al. (2010) were restricted to rates equivalent to a threshold of 9000 flashes per hour. They found an LNO_x – flash correlation coefficient of only 0.04 and PEs less than 15 mol per flash in ~half of their examined cases. These values are consistent with the present study at comparably high flash rates.

5.2 Geophysical implications

Studies have suggested PE may be directly related to flash size, with larger flashes producing more LNO_x (Huntrieser, et al., 2008; Carey et al., 2014; Marais et al., 2018). During the TROCCINOX campaign, Huntrieser et al. (2008) attributed lower tropical PE values to shorter stroke lengths relative to those of midlatitude storms. The effect of flash extent and LNO_x production was quantified by Carey et al. (2014). They applied the NASA Lightning Nitrogen Oxides Model (LNOM) (Koshak et al., 2014) to observations made during the Deep Convective Cloud and Chemistry (DC3) campaign and computed LNO_x production per meter of channel length from a Lightning Mapping Array, based on laboratory measurements and theoretical assumptions. They found LNO_x production to be highly correlated with flash extent (correlation coefficient of r = 0.99), indicating the PE is controlled almost entirely by the flash size.

Evidence from field campaigns have also shown a relationship between flash rate, flash size and updraft strength. In a study of two 2004 supercells, Bruning and MacGorman (2013) reported that increasing updraft strength is associated with smaller flash extents and higher average flash rates. Similar associations were noted by Carey et al. (2005), Kuhlman et al. (2009) and Weiss et al. (2012), as well as studies from the Deep Convective Cloud and Chemistry (DC3) campaign (Carey et al., 2014; Barth et al., 2015; Mecikalski et al., 2015; Bruning and Thomas, 2015). Bruning and Thomas (2015) demonstrated the anti-correlation between flash rate and size is strongest during the decay phase of the storm as the updraft weakens and flash rates drop, while the total energy from lightning diminishes. Marais et al. (2018) noted a stronger correlation of LNO_x with flash extent than with flash duration or radiance, implying the dependence of flash extent on flash rate may be the dominant factor driving the PE dependence on flash rate, consistent with Carey et al. (2014). Together, the above studies provide a possible geophysical basis for the dependence of PE on flash rate found in the present investigation.

CTMs parameterize LNO_x production with the assumption that midlatitude flashes produce more NO per flash than tropical flashes based on analyses of data from field campaigns (Hudman et al., 2007; Allen et al., 2010; Ott et al., 2010; Murray et al., 2012). The contention of Huntrieser et al. (2008) that higher midlatitude PEs are related to longer midlatitude strokes was based, in part, on speculation that the stronger wind shear in that region generates longer flashes. However, this hypothesis is contradicted by the association between stronger wind shear and stronger updrafts (e.g. Markowski and Richardson, 2011). These updrafts yield more frequent, but smaller less productive flashes, as noted above. Our midlatitude PE of 180 ± 100 may be compared with the somewhat smaller tropical value of 133 ± 72 mol per flash from Allen et al. (2019), since both were obtained similarly. The values are consistent with midlatitude flashes being more productive; however, the difference between these midlatitude and tropical PEs is not significant statistically due to the relatively high uncertainties. This conclusion is corroborated by Marais et al. (2018), who found no significant difference between mid- and tropical latitudes and noted that the higher GEOS-Chem midlatitude PE of 500 mol per flash overestimated observed OMI NO_2. Nonetheless, the tropical boreal summer values of Allen et al. and the present study can be combined to extrapolate an adjusted mean global production rate for the boreal summer. Weighting by a ~3:1 ratio of tropical to midlatitude flashes (Christian et al.,

2003) yields an adjusted rate of 2.9 ± 1.6 Tg N/yr, or 78% of the midlatitude extrapolation. While this rate is only based on measurements from the boreal summer, it is smaller than but within the uncertainty range of the Schuman and Huntrieser (2007) value of 5 ± 3 Tg N/yr.

5.3 Algorithm comparisons

We examine four OMI-based studies to illustrate how derived PEs can be extremely sensitive to algorithmic assumptions, even when using comparable data sets. The PE estimates of Pickering et al. (2016) for the Gulf of Mexico and Allen et al. (2019) in the tropics are based on OMI NO_2 and WWLLN lightning data, although Pickering et al. (2016) employed a significantly different approach. The algorithm in the Allen et al. study is more similar to that of the present approach although there are some differences, including a modified stratospheric estimate and a derivation of mean PE by linear regression. Their summation and regression analyses yielded average tropical PEs of 107 and 159 mol per flash, respectively, with a mean value of 133 ± 72 mol per flash. As noted, Allen et al. found that, on a regional basis, PE decreases with flash rate.

Pickering et al. (2016) also combined regression and summation to obtain the much smaller mean PE of 80 ± 45 mol per flash over the Gulf of Mexico, and 84 mol per flash estimated by summation only. We applied the present algorithm to the Gulf region and obtained 148 mol per flash. Beginning with this value, the differences in the Pickering et al. algorithm were then applied sequentially to demonstrate their relative impacts, expressed as multiplicative factors. The differences are (1) NASA OMI NO_2 v2.1 instead of v3 (1.04 – see Krotkov et al., 2017), (2) WWLLN flash version of Pickering et al., instead of the Allen et al. update (1.48), (3) a 3-hour flash window instead of 1 hour (0.65), (4) a 3-day LNO_x lifetime instead of 3-hours (0.62), (5) an unsmoothed stratosphere (0.80), (6) an 18% tropospheric background instead of the present OMI-data-based approach (3.00), (7) a 1000 flash per hour threshold (0.39). The net effect of these factors is a combined factor of 0.568. Multiplied by the initial 148 mol per flash derived with the present method, it yields a PE of 86 mol per flash, which is approximately the Pickering et al. summation value.

In their LNO_x study, Marais et al. (2018) used climatological NO_2 and lightning data to derive a PE of 280 ± 80 mol per flash. Seasonal mean OMI LNO_x columns from the v3 NASA OMI standard product were obtained by cloud slicing (Ziemke et al., 2001; Choi et al., 2014), with an OCP range of 280 – 450 hPa and no explicit adjustment for LNO_2 below OCP. Since climatological data represents ambient NO_x, accumulated from multi-year lightning activity, no background subtraction is used. The 2006 – 2008 OMI data were divided into geographic regions $20^o \times 32^o$ in longitude and latitude and compared with a lightning climatology from OTD/LIS, which was also used in the present study to calibrate the WWLLN counts. The PE was estimated by constraining the LNO_x source strength in GEOS-Chem to best fit the OMI cloud-sliced NO_2 observations. Unlike the present study, they made no correction for a model discrepancy in the NO/NO_2 ratio relative to aircraft data (see section 5.5), which could partially account for their relatively high PE. Because of the above differences, comparison of our mean PE with theirs is more challenging than with Pickering et al. (2016) and Allen et al. (2019).

Bucsela et al. (2010) examined four convective systems during TC^4. Estimated PEs from each, ranged from 87 to 246 mol per flash, with a mean value and uncertainty of 174 ± 219 mol per flash. Their flash counts were obtained from WWLLN on three of the days and CRLDN on one, with NO_2 data from the v1.0 NASA OMI NO_2 standard product. The latter included tropospheric AMFs and a wave-2 stratosphere, modified for the purpose of their study. The A_{LNOx} was based on a measured composite LNO_2 profile and GMI photolysis ratios. As in the present study, tropospheric backgrounds were estimated from convection-free days during the experiment. However, the outflow regions analyzed were not restricted to those with high cloud fractions, and this potentially compromised the accuracy of their background estimate. Their average tropical PE of 174 mol per flash is similar to the present midlatitude value, but the uncertainty is large, and it is based on a limited number of events.

5.4 Stratospheric estimate

Stratospheric NO_2 is the largest component of the total NO_2 column, constituting ~95% of the NO_2 vertical column for all grid boxes and ~85% for boxes with >5000 flashes per hour. Zonal smoothing of the NASA OMI NO_2 stratosphere mitigates aliasing of parts of the tropospheric signal into the stratosphere (Bucsela et al., 2013; Beirle et al., 2016; Allen et al., 2019). Although the smoothing does alias stratospheric features that depart from the zonal mean into the troposphere, these departures have a mean value of ~0 and do not bias the average PE. Figure 12 shows mean V_{init} and mean stratospheric NO_2 with and without zonal smoothing as a function of flash rate. V_{init} increases by ~0.5×10^{15} molecules cm^{-2} as the flash rate increases from ~0 to ~12,000 flashes per hour. Over the same range, $V_{StratZonal}$ increases slightly by 0.04×10^{15}. However, V_{strat} shows a larger increase of 0.15×10^{15} as the flash rate increases due to stratospheric aliasing of LNO_2. The difference in the mean values of V_{strat} for boxes with a flash rate of zero, which are used for the background estimate, and the values in flashing boxes introduce a low bias in LNO_x and PE for the unsmoothed stratosphere. The PE derived from the latter is 120 mol per flash, which is ~30% lower than that derived from a zonally smoothed stratosphere.

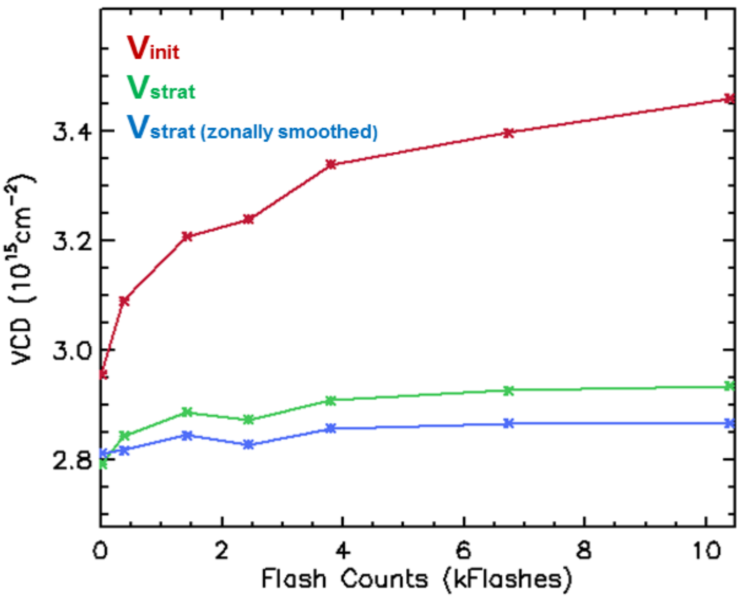

Figure 12: Dependence of average V_{init}, V_{strat} and $V_{StratZonal}$ (1×10^{15} molecules cm^{-2}) on 1-hour flash counts. All data have CRF > 0.97 and OCP < 500 hPa.

5.5 Estimate of uncertainty in the average PE

The sensitivity of the PE to algorithmic assumptions was used to quantify systematic errors, which are the main components of the error budget. Statistical errors in OMI and WWLLN data were found to be negligible, as in Bucsela et al. (2010). We discuss the error sources individually and combine them to obtain a net uncertainty in the mean PE.

5.5.1 Stratosphere

To test the effects of stratospheric column errors, a uniform bias of $\pm 2 \times 10^{14}$ cm^{-2} was applied to the zonally smoothed stratosphere. The magnitude of this bias is in line with previous stratospheric NO_2 uncertainty estimates (Boersma et al., 2004, 2007; Bucsela et al., 2006). It is twice the error assumed by Allen et al. (2019) and Bucsela et al (2010) in the tropics, where stratospheric columns are approximately half those at midlatitude, and the absolute uncertainty is assumed to be smaller. A ±2 $\times 10^{14}$ cm^{-2} error is 5 – 10% of the total midlatitude NO_2 column, ~90% of which is stratospheric. However, its effect on PE is only ±14% since it is uniform and is partially canceled in the background subtraction. Without background subtraction, the stratospheric bias would have a > 90% effect on PE. The stratospheric component of the PE error is taken to be ±15%.

5.5.2 Transport and chemistry effects

In this study, all LNO_x from lightning in the 1-hour integration period before OMI overpass is assumed to be accounted for in the retrieval and full correction made for contamination by ambient NO_x. This assumption is affected by errors in estimates of lofted pollution, LNO_x lifetime, advection and background. The 3-hour lifetime for LNO_x in near-field of convection (Nault et al., 2017) is shorter than previous estimates of ~2 – 8 days (Jaeglé et al., 1998, Martin et al., 2007; Schumann and Huntrieser, 2007), which would make chemical loss negligible. B. Nault (private communication) gives an uncertainty range in his lifetime of 2 to 12 hours, which for a 1-hour window introduces a PE uncertainty of ±10%. For boundary layer contamination, we assume a possible range of 10 – 20% for lofted pollution (DeCaria et al., 2000; 2005), which brackets our 15% downward adjustment in PE by ±5%.

Advection of LNO_x from flashing boxes could result in a negative PE bias. If upper tropospheric wind speeds are ~16 m/sec (a reasonable value for the midlatitudes in summer), a simple calculation shows that approximately 30% of the LNO_x would be advected out of the box during the hour before measurement, with a reduction in PE by the same amount. The net loss would be lower if advection into the boxes from upwind sources compensates for some of the loss. The amount of this loss may also be estimated by comparing PEs derived from flashes over 1-hour and 2-hour intervals. Assuming an accurate NO_x, higher flash rates over a longer window should be offset by a smaller background, with minimal net effect on PE. It was found that the PE based on 2-hour flashes is 15% smaller than the PE derived from 1-hour flashes. We attribute this difference mainly to advection. Overall, we estimate advection introduces a potential negative bias in PE of ~20% and assume an uncertainty of ±10%.

The mean midlatitude background estimated from non-flashing boxes is 55 ±10% of total LNO_x*, where the uncertainty is the standard deviation of inter-annual variability. This is ~3 times the *a priori* 18 ±15% background of Pickering et al. (2016) in the Gulf of Mexico. It is comparable to the 50 ±15% of Allen et al. (2019), who derived their background from days without lightning, as in the present study, but imposed the additional restriction that adjacent boxes also contain no flashes. The ±10% background error here propagates as a PE uncertainty of ±15%. Background days not only lack flashes during the 1-hour flash-integration window, but also contain relatively few flashes during preceding hours. As such, even though they meet the CRF and OCP criteria used in this study, they may represent a less convectively active environment than that of flashing boxes, which are more likely to have flashes preceding the integration window. This may introduce a bias in the background, and therefore PE, although the effect is difficult to quantify. We assign an uncertainty of ±20%, which is less than the ±30% uncertainty obtained by Allen et al. (2019), who based their value on the sensitivity of PE to uncertainties in the y-intercept of their regression-based estimate of PE.

5.5.3 NO_2 profiles

Retrieved LNO_x* is inversely proportional to the air mass factor A_{LNOx} in Equation (1). Beirle et al. (2009; 2010) estimated AMFs for a variety of storm environments and found that a fixed average AMF of 0.46 was adequate for their LNO_x retrievals from SCIAMACHY NO_2 data. We find this value reasonable, since substitution of the Beirle et al. AMF decreased the present PE by only 13%. The AMF is computed with GMI *a priori* NO_2 and NO_x profile shapes from days with the 3rd largest LNO_x column in a given month but is relatively insensitive to the rank within the month. Using the 1st or 10th largest columns changed the PE by only ~5%. Midlatitude simulations put 10 – 15% of LNO_x at altitudes below 600 hPa, ~20% below 500 hPa, and ~30% below 400 hPa. Between OCP thresholds of 400 and 600 hPa, the average PE varies by ±12%. We adopt a net PE uncertainty of ±15% due to errors in profile shape and OCP threshold.

The partitioning of NO_x into NO and NO_2 in GMI/GEOS-Chem, which affects the AMF, has been re-examined recently by Travis et al. (2016) and Silvern et al. (2018). They found GEOS-Chem NO/NO_2 ratios near and above 10 km to be approximately a factor of 2 larger than those of *in situ* measurements from the SEAC^{4}RS campaign. Travis et al. (2016) attribute this to model underestimation of HO_2 and RO_2, but Silvern et al. (2018) suggest that their required model adjustments of peroxy radicals are inconsistent with observations. Instead, Silvern et al. (2018) posit a combination of model errors in the NO_2-to-NO photolysis rate and the NO + O_3 reaction rate, k_1, along with possible bias in the *in situ* data due to a neglected labile NO_x reservoir. They noted that a k_1 increase of a factor of 1.4 and a photolysis rate decrease of 20% reduced the model NO/NO_2 by ~40%. The net effect is a ~28% reduction in NO_x/NO_2 and hence an increase in A_{LNOx} with a corresponding 28% decrease in PE. However, given that their factor of 1.4

represents a ~2σ change in k_1, that there are also possible significant measurement interferences, and that Silvern et al. and Travis et al. are relatively recent studies, we account for the potential error as a 20% high bias with a ±15% uncertainty.

5.5.4 WWLLN DE

The WWLLN flash counts are the largest source of PE uncertainty. Pickering et al. (2016) estimated a ±30% uncertainty in their WWLLN counts for the Gulf of Mexico, based on two independent schemes for estimating the DE, which differed by 25 – 30%. Their DEs were ~10 – 25% in the years 2007 – 2011. Citing NALMA data, Allen et al. (2019) questioned whether the Pickering et al. ±30% was too low, given the small size of the Gulf region and the temporal variation of their DEs. In their tropical study, Allen et al. assigned uncertainties to the WWLLN data proportional to area-size and WWLLN DE. Adopted values were ±25% over the tropics as a whole and ±30-50% for sub-regions that included tropical parts of the Americas, Africa and the Pacific, as well as the Gulf of Mexico. The mean area-weighted DE for the tropics was ~13%, and the entire geographic area covered was 2.6×10^8 km^2. In the present study, the mean area-weighted DE is ~6% over our total geographic area of 0.6×10^8 km^2. Based on these considerations, we assign a conservative uncertainty of ±45% to our WWLLN flash counts.

5.5.5 Net uncertainty

The net uncertainty in average PE combines the major sources of systematic error summarized in Table 2. Following Bucsela et al. (2010), Pickering et al. (2016) and Allen et al. (2019), the systematic errors are added in quadrature. Biases are the change in PE resulting from neglect of an error source. The WWLLN detection efficiency contributes an error of ±45%, and the remaining uncertainties are ±20% or less. These include the stratospheric component: ±15%, LNO_x chemical decay: ±10%, lofted pollution: ±5%, advection loss: –20 ± 10%, NO_x background: ±20%, OCP threshold and error in the below-cloud amount: ±15%, and the UT NO/NO_x: 20 ±15%. Net positive and negative biases are equal in magnitude and so have no net effect on average PE. And additional source of error is the NO_2 slant columns (Krotkov et al., 2017;, Zara et al., 2017; Allen et al., 2019). This error is included as a ±5% uncertainty. The resulting uncertainty is ±58%.

Table 2:

Potential biases and errors in the average PE estimate.

Source	Bias ± error (%)	Bias ± error (mol per flash)
Stratosphere	0 ± 15	0 ± 27
NO_x lifetime	0 ± 10	0 ± 18
Lofted pollution	0 ± 5	0 ± 9
Advection loss	–20 ± 10	–36 ± 18
Tropospheric background	0 ± 20	0 ± 36
OCP and below-cloud LNO_x	0 ± 15	0 ± 27
NO / NO_2 ratio	20 ± 15	36 ± 27
WWLLN detection efficiency	0 ± 45	0 ± 81
NO_2 slant columns	0 ± 5	0 ± 9
Net PE bias and uncertainty	0 ± 58	0 ± 100

6. Conclusions

The production efficiency of LNO_x and its apparent dependence on flash rate have been explored with OMI NO_2 and WWLLN lightning measurements. The midlatitude dataset and algorithm used here are similar to those of the tropical study of Allen et al. (2019). The Gulf of Mexico study of Pickering et al. (2016) was also based on OMI and WWLLN data but employed a different approach. We obtain an average summertime northern midlatitude PE of 180 ± 100 mol per flash. The average PEs of Allen et al. (2019) and Pickering et al. (2016) were 133 ± 72 and 80 ± 45 mol per flash, respectively. While smaller, the Allen et al. value is equivalent to the present result within the studies' uncertainties and does not provide compelling evidence of a systematic difference in PE between the tropics and midlatitudes. This finding was also reported by Marais et al. (2018), who obtained a significantly larger PE of 280 mol per flash. However, their use of climatological NO_2 data from cloud slicing and an OTD/LIS lightning climatology in constraining the GEOS-Chem model differs from the present study and complicates direct comparisons with our results. Pickering et al.'s smaller 80 mol per flash is also attributable to algorithmic differences, particularly involving tropospheric background estimation, flash-rate threshold and NO_x lifetime. Their high flash-rate threshold and that of Beirle et al. (2010), are consistent with the small and, in some cases negligible, PEs found in those studies, given the strong inverse relationship between PE and flash rate that we have shown here.

We find an approximate power-law relationship between the rates of LNO_x production and flashes, corresponding to a PE that decreases by an order of magnitude when flash rate is increased by ~2 orders of magnitude. A slightly weaker dependence of PE on flash rate is seen over convective clouds having an OCP < 400 hPa. A possible mechanism for the decrease in PE with flash rate may be inferred from several LMA studies showing that flash size and flash rate are also inversely correlated (e.g. Bruning and Thomas, 2015). The flash-rate dependence implies a need for caution when extrapolating PE values from limited datasets to estimate global LNO_x production. For such estimates, flash rate and size distributions must be taken into account. However, if northern midlatitude distributions are representative of those globally, then our average estimate of 180 ± 100 mol per flash is equivalent to 3.5 ± 2.0 Tg N/yr, LNO_x or roughly 16% of total global NO_x production. A flash-count-weighted average of our midlatitude PE and Allen et al.'s tropical PE yields a global production rate of 2.9 ± 1.6 Tg N/yr for the boreal summer months.

Future satellite missions with improved instrumentation and temporal coverage will help verify and/or refine the present PE. In particular, the Tropospheric Monitoring Instrument (TROPOMI) is providing NO_2 measurements unaffected by OMI's row anomaly and at higher spatial resolution (3.5 x 7 km^2) from low earth orbit (Veefkind et al., 2012). For observations spanning the afternoon diurnal peak of convection, geostationary instruments are needed. The Tropospheric Emissions: Monitoring of Pollution (TEMPO) instrument (Zoogman et al., 2017) and Geostationary Environment Monitoring Spectrometer (GEMS) (Kim, 2012) will be such instruments. Their data can be combined with continuous DE-adjusted flash counts from the GOES-16 and GOES-17 Geostationary Lightning Mapper (GLM) instruments (Goodman et al., 2013).

Acknowledgments

This research was funded under the NASA Aura Science Team. We thank Megan Damon of Science Systems and Applications, Inc. for GMI simulations. The authors wish to thank the World Wide Lightning Location Network (http://wwlln.net), a collaboration among over 50 universities and institutions, for providing the lightning location data used in this paper. WWLLN data for June-August 2007 - 2011 are available from the University of Washington. Please see http://wwlln.net/new/ for more information. Data sets of relative detection efficiencies are available at http://wwlln.net/deMaps/. Upon acceptance of this journal article, the OMI data and IDL readers used in this study will be archived and accessible via open web access on a University of Maryland department server.

References

Abarca, S. F., Corbosiero, K. L., & Galarneau, T. J. Jr., (2010), An evaluation of the World Wide Lightning Location Network (WWLLN) using the National Lightning Detection Network (NLDN) as ground truth, *Journal of Geophysical Research: Atmospheres*, **115**, D18206, doi:10.1029/2009JD013411.

Acarreta, J. R., deHaan, J. F., & Stammes, P. (2004), Cloud pressure retrieval using the O_2-O_2 absorption band at 477 nm, *Journal of Geophysical Research: Atmospheres*, vol. 109, D05204, doi:10.1029/2003JD003915.

Allen, D. J., Pickering, K. E., Duncan, B., & Damon, M. (2010), Impact of lightning NO 859 emissions on North American photochemistry as determined using the Global Modeling 860 Initiative (GMI) model, *Journal of Geophysical Research: Atmospheres*, 115, D22301, 861 doi:10.1029/2010JD014062.

Allen, D. J., Pickering, K. E., Pinder, R. W., Henderson, B. H., Appel, K. W., Prados, A. (2012), Impact of lightning-NO on eastern United States photochemistry during the summer of 2006 as determined using the CMAQ model, *Atmospheric Chemistry and Physics*, 12(4), 1737–1758, doi:10.5194/acp-12-1737-2012.

Allen, D. J., Pickering, K. E., Bucsela, E., Krotkov, N., Holzworth, R. (2019), Lightning NO_x Production in the Tropics during the boreal summer as Determined Using OMI NO_2 Retrievals and WWLLN Stroke data, J. *Geophysical Research: Atmospheres*, submitted.

Barth, M., et al. (2015), The Deep Convective Clouds and Chemistry (DC3) field campaign, *Bulletin of the American Meteorological Society*,doi:10.1175/BAMS-D-13-00290.1.

Beirle, S., Spichtinger, N., Stohl, A., Cummins, K. L., Turner, T., Boccippio, D., Cooper, O. R., Wenig, M., Grzegorski, M., Platt, U., & Wagner, T. (2006). Estimating the NOx produced by lightning from GOME and NLDN data: a case study in the Gulf of Mexico, *Atmospheric Chemistry and Physics*, **6**, 1075-1089.

Beirle, S., Salzmann, M., Lawrence, M. G., & Wagner, T. (2009), Sensitivity of satellite observations for freshly produced lightning NOx, *Atmospheric Chemistry and Physics*, 9, 1077-1094, https://doi.org/10.5194/acp-9-1077-2009.

Beirle, S., Huntrieser, H., & Wagner T. (2010), Direct satellite observation of lightning-produced NO_x, *Atmospheric Chemistry and Physics*, 10, 18255–18313, 2010, doi:10.5194/acpd-10-18255-2010.

Beirle, S., Koshak, W., Blakeslee, R., & Wagner, T. (2014), Global patterns of lightning properties derived from OTD and LIS, *Natural Hazards and Earth System Sciences*,14, 2715-2726. https://doi.org/10.5194/nhess-14-2715-2014.

Beirle, S., Hörmann, C., Jöckel, P., Penning de Vries, M., Pozzer, A., Sihler, H., Valks, P., & Wagner, T. (2016), The STRatospheric Estimation Algorithm from Mainz (STREAM): Estimating stratospheric NO_2 from nadir viewing satellites by weighted convolution, *Atmosphere Measurement Technical Discussion*, doi:10.5194/amt-2015-405.

Bhetanabhotla, M. N., Crowell, B. A., Coucouvinos, A., Hill, R. D., & Rinker, R. G. (1985), Simulation of trace species production by lightning and corona discharge in moist air, *Atmospheric Environment*, 19, 1391–1397.

Boccippio, D. J., Koshak, W., Blakeslee, R., Driscoll, K., Mach, D., Buechler, D., et al. (2000). The Optical Transient Detector (OTD): Instrument characteristics and cross-sensor validation, *Journal of Atmospheric and Oceanic Technology*, 17(4), 441-458.

Boccippio, D.J., Koshak, W., & Blakeslee, R. (2002). Performance assessment of the Optical Transient Detector and Lightning Imaging Sensor. Part I: Predicted Diurnal Variability, *Journal of Atmospheric and Oceanic Technology*, 19, 1318-1332.

Boersma, K. F., Eskes, H. J., Brinksma, E. J. (2004), Error analysis for tropospheric NO_2 from space, *Journal of Geophysical Research: Atmospheres*, 109, D04311, doi:10.1029/2003JD003962.

Boersma, K. F., Eskes, H. J., Meijer, E. W., & Kelder, H. M. (2005), Estimates of lightning NOx production from GOME satellite observations, *Atmospheric Chemistry and Physics*, 5, 2311-2331.

Boersma, K.F., Eskes, H. J., Veefkind, J. P., Brinksma, E. J., van der A, R. J., Sneep, A. M., van den Oord, G. H. J., Levelt, P. F., Stammes, P., Gleason, J. F., and Bucsela, E. J., (2007), Near-real time retrieval of tropospheric NO_2 from OMI, *Atmospheric Chemistry and Physics*, 7, 2103-2118.

Boersma, K. F., Eskes, H. J., Dirksen, R. J., van der A, R. J., Veefkind, J. P., Stammes, P., Juijnen, V., Kleipool, Q. L., Sneep, M., Claas, J., Leitao, J., Richter, A., Zhou, Y., & Brunner, D. (2011), An improved tropospheric NO_2 column retrieval algorithm for the Ozone Monitoring Instrument, *Atmospheric Measurement Techniques*, 4, 2329-2388, doi:10.5194/amtd-4-2329-2011.

Bruning, E. C., & MacGorman, D. R. (2013), Theory and observations of controls on lightning flash size spectra, *Journal of the Atmospheric Sciences*, 70(12), 4012–4029, doi:10.1175/JAS-D-12-0289.1.

Bruning, E. C., & Thomas, R. J. (2015), Lightning channel length and flash energy determined from moments of the flash area distribution, *Journal of Geophysical Research: Atmospheres*, 120, doi:10.1002/2015JD023766.

Bucsela, E.J., Celarier, E. A., Wenig, M. O., Gleason, J. F., Veefkind, J. P., Boersma, K. F., and Brinksma, E. (2006), Algorithm for NO_2 vertical column retrieval from the Ozone Monitoring Instrument, *IEEE Transactions on Geoscience and Remote Sensing*, **44**, 1245-1258.

Bucsela, E. J., Pickering, K. E., Huntemann, T. L., Cohen, R. C., Perring, A., Gleason, J. F., Blakeslee, R. J., Albrecht, R. I., Holzworth, R., Cipriani, J. P., Vargas-Navarro, D., Mora-Segura, I., Pacheco-Hernández, A., and Laporte-Molina, S. (2010), Lightning-generated NOx seen by the Ozone Monitoring Instrument during NASA's Tropical Composition, Cloud and Climate Coupling Experiment (TC^4), *Journal of Geophysical Research: Atmospheres*, **115**, D00J10, doi:10.1029/2009JD013118.

Bucsela, E. J., Krotkov, N. A., Celarier, E. A., Lamsal, L. N., Swartz, W. H., Bhartia, P. K., Boersma, K. F., Veefkind, J. P., Gleason, J. F., & Pickering, K. E. (2013), A new stratospheric and tropospheric NO_2 retrieval algorithm for nadir-viewing satellite instruments: applications to OMI, *Atmospheric Measurement Techniques*,6, 2607-2626, doi:10.5194/amtd-6-2607-2013.

Carey, L.D., Murphy, M. J., McCormick, T. L., & Demetriades, N. W. (2005), Lightning location relative to storm structure in a leading line trailing stratiform mesoscale convective system. *Journal of Geophysical Research: Atmospheres*, 110, D03105, doi:10.1029/2003JD004371.

Carey, L. D., Koshak, W., Peterson, H., Matthee, R., & Bain, A. L. (2014), The kinematic and microphysical control of lightning rate, extent and NO_x production, *XV International Conference on Atmospheric Electricity*, June 2014, Norman Oklahoma.

Cecil, D. J., Buechler, D. E., Blakeslee, R. J. (2014), Gridded lightning climatology from TRMM-LIS and OTD: Dataset description, *Atmospheric Research*, 135-136, 404-414.

Choi, S., Joiner, J., Choi, Y., Duncan, B., Vasilkov, N., Krotkov, N., & E. Bucsela (2014), First estimates of global NO_2 abundances derived using a cloud-slicing technique applied to satellite observations from the Aura Ozone Monitoring Instrument (OMI), *Atmospheric Chemistry and Physics* 14, 10565-10588, doi: 10.5194/acp-14-10565-2014.

Christian, H. J., Blakeslee, R., J., Boccippio, D. J., Boeck, W. L., Buechler, D. E., Driscoll, K. T., Goodman, S. J., Hall, J. M., Koshak, W. J., Mach, D. M., Stewart, M. F. (2003), Global frequency and distribution of lightning as observed from space by the Optical Transient Detector, Journal of Geophysical Research: Atmospheres, 108, D1, 4005, doi:10.1029/2002JD002347.

Chronis, T., Koshak, W., & McCaul, E. (2016). Why do oceanic negative cloud-to-ground lightning exhibit larger peak current values?, *Journal of Geophysical Research: Atmospheres Atmos*., 121, 4049–4068, https://doi.org/10.1002/2015JD024129.

Cook, D. R., Liaw, Y. P., Sisterson, D. L., & Miller, N. L. (2000), Production of nitrogen oxides by a large spark generator, *Journal of Geophysical Research: Atmospheres*, 105, 7103–7110, doi:10.1029/1999JD901138.

Cooper, O., et al. (2006). Large upper tropospheric ozone enhancements above midlatitude North America during summer: In situ evidence from the IONS and MOZAIC ozone measurement network. *Journal of Geophysical Research: Atmospheres*, 111(D24).

Cooper, O. R., et al. (2007), Evidence for a recurring eastern North America upper tropospheric ozone maximum during summer, *Journal of Geophysical Research: Atmospheres*, 112 (D23).

Cummings, K. A., Huntemann, T. L., Pickering, K. E., Barth, M. C., Skamarock, W. C., Holler, H., Betz, H.-D., Volz-Thomas, A., & Schlager, H. (2013), Cloud-resolving chemistry simulation of a Hector thunderstorm, *Atmospheric Chemistry and Physics*, 13, 2737-2777, 989 doi:10.5194/acp-13-2757-2013.

Dahlmann, K., Grewe, V., Ponater, M., & Matthes, S. (2011), Quantifying the contributions of individual NOx sources to the trend in ozone radiative forcing, *Atmospheric Environment*, 45, 2860–2868, https://doi.org/10.1016/j.atmosenv.2011.02.071.

Davé, J.V. (1965), Multiple scattering in a non-homogeneous, Rayleigh atmosphere, *Journal of the Atmospheric Sciences*, 22, 273-279.

DeCaria, A. J., Pickering, K. E., Stenchikov, G. L., Scala, J. R., Stith, J. L., Dye, J. E., et al. (2000), A cloud-scale model study of lightning-generated NOx in an individual thunderstorm during STERAO-A, *Journal of Geophysical Research: Atmospheres*, 105(D9), 11601–11616, https://doi.org/10.1029/2000JD900033

DeCaria, A. J., Pickering, K. E., Stenchikov, G. L., & Ott, L. E. (2005), Lightning-generated NO_x and its impact on tropospheric ozone production: A three-dimensional modeling study of a Stratosphere-Troposphere Experiment: Radiation, Aerosols, and Ozone (STERAO-A) thunderstorm, *Journal of Geophysical Research: Atmospheres*, 110, D14303, https://doi.org/10.1029/2004JD005556.

Dobber, M., Kleipool, Q., Dirksen, R., Levelt, P., Jaross, G., Taylor, S., Kelly, T., Flynn, L., Leppelmeier, G. & Rozemeijer, N. (2008), Validation of Ozone Monitoring Instrument level 1b data products, *Journal of Geophysical Research: Atmospheres,*113(D15), D15S06, doi:10.1029/2007JD008665.

Dowden, R. L., Brundell, J. B., & Rodger, C. J. (2002), VLF lightning location by time of group 394 arrival (TOGA) at multiple sites. *Journal of Atmospheric and Solar-Terrestrial Physics*, 64, 817-830.

Duncan, B. N., Strahan, S. E., Yoshida, Y., Steenrod, S. D., & Livesey, N. (2007), Model study of the cross-tropopause transport of biomass burning pollution, *Atmospheric Chemistry and Physics*, 7, 3713-3736.

Finlayson-Pitts, B. J. & Pitts, J. N. Jr. (1999), *Chemistry of the Upper and Lower Atmosphere*, Academic Press, ISBN 012257060X.

Fiore, A. M., L. W. Horowitz, E. J. Dlugokencky, and J. J. West (2006), Impact of meteorology and emissions on methane trends, 1990–2004, *Geophysical Research Letters*, 33, L12809, doi:10.1029/2006GL026199.

Gallardo, L., & Cooray, V. (1996), Could cloud-to-cloud discharges be as effective as cloud-to-ground discharges in producing NO_x?, *Tellus*, 4b, 641-651.

Goodman, S. J., Blakeslee, R. J., Koshak, W. J., Mach, D., Bailey, J., Buechler, D., Carey, L., Schultz, C., Bateman, M., McCaul, E., Jr., Stano, G., (2013), The GOES-R Geostationary Lightning Mapper (GLM), *Atmospheric Research*, 125-126, 34-49.

Hudman, R. C. et al. (2007), Surface and lightning sources of nitrogen oxides over the United States: Magnitudes, chemical evolution, and outflow, *Journal of Geophysical Research: Atmospheres Atmos*., 112, D12S05, doi:10.1029/2006JD007912.

Huntrieser, H., Schlager, H., Hoeller, H., Schumann, U., Betz, H. D., Boccippio, D., Brunner, D., Forster, C., and Stohl, A. (2006), Lightning-produced NOx in tropical, subtropical and midlatitude thunderstorms: New insights from airborne and lightning observations, *Geophysical Research Abstracts*, 8, 03286, SRef-ID:1607-7962/gra/EGU06-A-03286.

Huntrieser, H., Schumann, U., Schlager, H., Höller, H., Giez, A., Betz, H.-D., Brunner, D., Forster, D., Pinto, O., Jr., & Calheiros, R. (2008), Lightning activity in Brazilian thunderstorms during TROCCINOX: implications for NO_x production, *Atmospheric Chemistry and Physics*, 8, 921-953.

Huntrieser, H., Schlager, H., Lichtenstern, M., Stock, P., Hamburger, T., Höller, H., Schmidt, K., Betz, H.-D., Ulanovsky, A., & Ravengnani, F. (2011), Mesoscale convective systems observed during AMMA and their impact on the NO_x and O_3 budget over West Africa, *Atmospheric Chemistry and Physics*, 11, 2503-2536.

Hutchins, M. L., Holzworth, R. H., Brundell, J. B., & Rodger, C. J. (2012), Relative detection efficiency of the World Wide Lightning Location Network, *Radio Science*, 47, RS6005, doi:10.1029/2012RS005049.

Jaeglé, L., Jacob, D. J., Wang, Y., Weinheimer, A. J., Ridley, B. A., Campos, T. L., Sachse, G. W., & Hagen, D. E. (1998), Sources and chemistry of NO in the upper troposphere over the United States, *Geophysical Research Letters*, 25, 1709 – 1 712.

Kim, J., S (2012), GEMS (Geostationary Environment Monitoring Spectrometer) onboard the GeoKOMPSAT to Monitor Air Quality in high Temporal and Spatial Resolution over Asia-Pacific Region, EGU *General Assembly 2012*, 22–27 April 2012, Vienna, Austria, p. 4051.

Kleipool Q. L., Dobber, M. R., de Haan, J. F., Levelt, P. F. (2008), Earth surface reflectance climatology from 3 years of OMI data, *Journal of Geophysical Research: Atmospheres*, **113**, D18308, doi:10.1029/2008JD010290.

Koshak, W. J., Solakiewicz, R. J., Blakeslee, R. J., Goodman, S. J., Christian, H. J., Hall, J. M., et al. (2004). North Alabama Lightning Mapping Array (LMA): VHF source retrieval algorithm and error analyses. *Journal of Atmospheric and Oceanic Technology, 21*(4), 543-558.

Koshak, W. (2014), Global Lightning Nitrogen Oxides Production, Chapter 19 of *The Lightning Flash*, 2nd edition, editor V. Cooray, ISBN: 978-1-84919-691-8, pp. 928.

Krotkov, N. A, Lamsal, L. N., Celarier, E. A., Swartz, W. H., Marchenko, S. V., Bucsela, E. J., Chan, K. L., Wenig, M. O., & Zara, M. (2017), The version 3 OMI NO2 standard product, *Atmospheric Measurement Techniques,*10, 3133- 3149, 2017, https://doi.org/10.5194/amt-10-3133-2017.

Kuhlman, K. M., Ziegler, C. L., Mansell, E. R., MacGorman, D. R., & Straka, J. M. (2006), Numerically simulated electrification and lightning of the 29 June 2000 STEPS supercell storm. *Monthly Weather Review*,134, 2734–2757.

Kumar, P. P., Manohar, G. K., & Kandalgaonkar, S. S. (1995), Global distribution of nitric oxide produced by lightning and its seasonal variation, *Journal of Geophysical Research: Atmospheres*, 100, 11 203–11 208.

Labrador, L.J., von Kuhlmann, R., & Lawrence, M.G. (2004), Strong sensitivity of the global mean OH concentration and the tropospheric oxidizing efficiency to the source of NOx from lightning, *Geophysical Research Letters*, 31, L06102, https://doi.org/10.1029/2003GL019229.

Lay, E. H., Holzworth, R. H., Rodger, C. J., Thomas, J. N., Pinto, O., & Dowden R. L. (2004), WWLLN global lightning detection system: Regional validation study in Brazil, *Geophysical Research Letters*,31, L03102, doi:10.1029/2003GL018882.

Levelt, P. F., Hilsenrath, E., Leppelmeier. G. W., van den Oord, G. B. J., Bhartia, P. K., Tamminen, J., de Haan, J. F., & Veefkind, J. P. (2006), Science Objectives of the Ozone Monitoring Instrument, *IEEE Transactions on Geoscience and Remote Sensing*,44(5), 1199–1208, doi:10.1109/TGRS.2006.872333.

Liaskos, C. E., Allen, D. J., & Pickering, K. E. (2015), Sensitivity of tropical tropospheric composition to lightning NOx production as determined by replay simulations with GEOS-5, *Journal of Geophysical Research: Atmospheres Atmos*., 120, 8512–8534, doi:10.1002/2014JD022987.

Marais, E. A., Jacob, D. J., Choi, S., Joiner, J., Belmonte-Rivas, M., Cohen, R. C., Beirle, S., Murray, L. T., Schiferl, L., Shah, V., & Jaeglé, L. (2018), Nitrogen oxides in the global upper troposphere: interpreting cloud-sliced NO_2 observations from the OMI satellite instrument, *Atmospheric Chemistry and Physics*, 18, 17017–17027, https://doi.org/10.5194/acp-18-17017-2018.

Marchenko, S., Krotkov, N. A., Lamsal, L. N., Celarier, E. A., Swartz, W. H., & Bucsela, E. J. (2015), Revising the slant column density retrieval of nitrogen dioxide observed by the Ozone Monitoring Instrument, *Journal of Geophysical Research: Atmospheres*, doi: 10.1002/2014JD022913.

Marchenko, S. V. & DeLand, M. T. (2014), Solar Spectral Irradiance changes during cycle 24, *The Astrophysical Journal*, 789(2), 117, doi: 10.1088/0004-637X/789/2/117.

Markowski, P. & Richardson, Y. (2011), Mesoscale Meteorology in Midlatitudes, John Wiley and Sons.

Martin, R. V., Chance, K., Jacob, D. J., Kurosu, T. P., Spurr, R. J. D., Bucsela, E., Gleason, J., Palmer, P. I., Bey, I., Fiore, A. M., Li, Q., Yantosca, R. M., & Koelmeijer, R. B. A. (2002), An improved retrieval of tropospheric nitrogen dioxide from GOME, *Journal of Geophysical Research: Atmospheres*, 107(D20), ACH9010ACH9-21, 4437, doi:10.1029/2001JD001027.

Martin, R. V., Sauvage, B., Folkins, I., Sioris, C. E., Boone, C., Bernath, P., & Ziemke, J. (2007), Space-based constraints on the production of nitric oxide by lightning, Journal of Geophysical Research: Atmospheres, 112, D09309, doi:10.1029/2006JD007831.

Mecikalski, R. M., Bain, A. L., & Carey, L. D. (2015), Radar and lightning observations of deep moist convection across northern Alabama during DC3: 21 May 2012, *Monthly Weather Review*, 143(7), 2774–2794, doi:10.1175/MWR-D-14-00250.1.

Miyazaki, K., Eskes, H. J., Sudo, K., & Zhang, C.: Global lightning NOx production estimated by an assimilation of multiple satellite data sets, Atmospheric Chemistry and Physics, 14, 3277–3305, doi:10.5194/acp-14-3277-2014, 2014.

Murray, L. T., Jacob, D. J., Logan, J. A. , Hudman, R. C. , & Koshak, J. W. (2012), Optimized regional and interannual variability of lightning in a global chemical transport model constrained by LIS/OTD satellite data, Journal of Geophysical Research: Atmospheres 117, doi: 10.1029/2012jd017934.

Nault, B. A., Laughner, J. L., Wooldridge, P. J., Crounse, J. D., Dibb, J., Diskin, G., Cohen, R. C. (2017), Lightning NOx Emissions: Reconciling Measured and Modeled Estimates With Updated NOx Chemistry, *Geophysical Research Letters*, 2017GL074436. doi:10.1002/2017GL074436.

Ott L. E., Pickering, K. E., Stenchikov, G. L., Huntrieser, H., & Schumann, U. (2007), Effects of lightning NOx production during the 21 July European Lightning Nitrogen Oxides Project storm studied with a three-dimensional cloud-scale chemical transport model, *Journal of Geophysical Research: Atmospheres*, **112**, D05307, doi:10.1029/2006JD007365.

Ott L. E., Pickering, K. E., Stenchikov, G. L., Allen, D. J., DeCaria, A. J., Ridley, B., Lin, R-F., Lang, S., & Tao, W-K (2010), Production of lightning NO_x and its vertical distribution calculated from three-dimensional cloud-scale chemical transport model simulations, *Journal of Geophysical Research: Atmospheres*, **115**, D04301, doi:10.1029/2009JD011880.

Peyrous, R. & Lapeyre, R. M. (1982), Gaseous products created by electrical discharges in the atmosphere and condensation nuclei resulting from gaseous phase reactions, *Atmospheric Environment*, 16, 959–968.

Pickering, K. E., Thompson, A. M., Tao, W. K., & Kucsera, T. L. (1993). Upper tropospheric ozone production following mesoscale convection during STEP/EMEX, *Journal of Geophysical Research: Atmospheres*, 98(D5), 8,737-8,749.

Pickering, K. E., Thompson, A. M., Wang, Y., Tao, W. K., McNamara, D. P., Kirchhoff, V. W., et al. (1996). Convective transport of biomass burning emissions over Brazil during TRACE A, *Journal of Geophysical Research: Atmospheres*, 101(D19), 23,993-24,012.

Pickering, K. E., Bucsela, E., Allen, D., Ring, A., Holzworth, R., & Krotkov, N. (2016), Estimates of lightning NO_x production based on OMI NO_2 observations over the Gulf of Mexico, *Journal of Geophysical Research: Atmospheres*, 121, 8668–8691, doi:10.1002/2015JD024179.

Price, C., Penner, J., & Prather, M. (1997), NO_x from lightning, 1. Global distributions based on lightning physics, *Journal of Geophysical Research: Atmospheres*, 102, 5929-5941.

Price, C., & Rind, D. (1992), A simple lightning parameterization for calculating global lightning distributions. *Journal of Geophysical Research: Atmospheres*, 97, 9919–9933.

Rap, A., Richards, N. A. D., Forster, P. M., Monks, S. A., Arnold, S. R., & Chipperfield, M. P. (2015), Satellite constraint on the tropospheric ozone radiative effect, *Geophysical Research Letters*, 42, 5074– 5081, https://doi.org/10.1002/2015gl064037.

Richter, A. & Burrows, J. P. (2002), Tropospheric NO2 from GOME measurements, *Advances in Space Research*, 29(11), 1673–1683, doi:10.1016/S0273-1177(02)00100-X.

Rienecker, M. M., et al. (2011), MERRA: NASA's Modern-Era Retrospective Analysis for Research and Applications, *Journal of Climate*, 24(14), 3624-3648, doi:10.1175/JCLI-D-00015.1.

Rodger C. J., Werner, S. W., Brundell, J. B., Thomson, N. R., Lay, E. H., Holzworth, R. H., & Dowden, R. L. (2006), Detection efficiency of the VLF World-Wide Lightning Location Network (WWLLN): Initial case study, *Annals of Geophysics*, 24, 3197-3214.

Rodger, C. J., Brundell, J. B., Holzworth, R. H., & Lay, E. H. (2009), Growing Detection Efficiency of the World Wide Lightning Location Network, *Am. Inst. Phys. Conf. Proc*., Coupling of thunderstorms and lightning discharges to near-Earth space: Proceedings of the Workshop, Corte (France), 23-27 June 2008, 1118, 15-20, DOI:10.1063/1.3137706.

Rudlosky, S.D. & Shea, D.T. (2013). Evaluating WWLLN performance relative to TRMM/LIS, *Geophysical Research Letters*, 40, 1-5, https://doi.org/10.1002/grl.50428

Schenkeveld, V M E., Jaross, G., Marchenko, S., Haffner, D., Kleipool, Q., Rozemeijer, N., Veefkind, J. P., & Levelt, P. F. (2017), In-flight performance of the Ozone Monitoring Instrument, *Atmospheric Measurement Techniques*; Katlenburg-Lindau Vol. 10, 1957 – 1986, doi:10.5194/amt-10-1957-2017.

Schoeberl, M.R., Douglass, A. R., Hilsenrath, E., Bhartia, P. K., Beer, R., Waters, J. W., Gunson, M., Froidevaux, L., Gille, J., Barnett, J., Levelt, P. F., & Decola, P. (2006), Overview of the EOS Aura Mission, *IEEE Transactions on Geoscience and Remote Sensing*, 44, 1066-1074.

Schumann, U. & Huntrieser, H. (2007), The global lightning-induced nitrogen oxides source, *Atmospheric Chemistry and Physics*, 7, 3823-3907.

Seinfeld, J. H., & Pandis, S. N. (1998), Atmospheric Chemistry and Physics: From air pollution to climate change, John Wiley & Sons, Inc, New York, 1998.

Schenkeveld, V M. E., Jaross, G., Marchenko, S., Haffner, D., Kleipool, Q. L., Rozemeijer, N., C., Veefkind, J. P., & Levelt, P. F., (2017), In-flight performance of the Ozone Monitoring Instrument, *Atmospheric Measurement Techniques,*10, 1957–1986, www.atmos-meas-tech.net/10/1957/2017/doi:10.5194/amt-10-1957.

Silvern, R. F., Jacob, D. J., Travis, K. R., Sherwen, T., Evans, M. J., Cohen, R. C., et al. (2018). Observed NO/NO2 ratios in the upper troposphere imply errors in NO-NO2-O3 cycling kinetics or an unaccounted NOx reservoir. *Geophysical Research Letters*, 45. https://doi.org/10.1029/2018GL077728.

Sneep, M., De Haan, J., Stammes, P., Wang, P., Vanbauce, C., Joiner, J., Vasilkov, A. P., & Levelt, P. F. (2008), Three-way comparison between OMI/Aura and POLDER/PARASOL cloud pressure products, *Journal of Geophysical Research: Atmospheres*, 113, D15S23, doi:10.1029/2007JD008694.

Stammes, P., Sneep, M., de Haan, J. F., Veefkind, J. P., Wang, P., & Levelt, P. F. (2008), Effective cloud fractions from the Ozone Monitoring Instrument: Theoretical framework and validation, *Journal of Geophysical Research: Atmospheres*, 113, D16S38, doi:10.1029/2007JD008820.

Strahan, S.E., Duncan, B. N., & Hoor, P. (2007), Observationally derived transport diagnostics for the lowermost stratosphere and their application to the GMI chemistry transport model, *Atmospheric Chemistry and Physics*, 7, 2435-2445.

Strahan, S. E., Douglass, A. R. & Newman, P. A. (2013), The contributions of chemistry and transport to low arctic ozone in March 2011 derived from Aura MLS observations, *Journal of Geophysical Research: Atmospheres: Atmospheres*, 118(3), 1563–1576, doi:10.1002/jgrd.50181.

Tost, H., Jckel, P., & Lelieveld, J. (2007), Lightning and convection parameterisations – uncertainties in global modelling, *Atmospheric Chemistry and Physics*, 7, 4553–4568, https://doi.org/10.5194/acp-7-4553-2007.

Travis, K. R., Jacob, D. J., Fisher, J. A., Kim, P. S., Marais, E. A., Zhu, L., Zhou, X. L. (2016). Why do models overestimate surface ozone in the Southeast United States? *Atmospheric Chemistry and Physics*, 16(21), 13561-13577. doi:10.5194/acp-16-13561-2016.

van der Werf, G. R., Randerson, J. T., Giglio, L., Collatz, G. J., Mu, M., Kasibhatla, P. S., Morton, D. C., DeFries, R. S., Jim, Y., & van Leeuwen, T. T. (2010), Global fire emissions and the contribution of deforestation, savanna, forest, agricultural, and peat fires (1997-2009), *Atmospheric Chemistry and Physics*, 10, 11,707-11,735.

van Donkelaar, A., Martin, R. V., Leaitch, W. R., Macdonald, A. M., Walker, T. W., Streets, D. G., Zhang, Q. , Dunlea, E. J., Jimenez, J. L., Dibb, J. E., Huey, L. G., Weber, R., & Andreae, M. O. (2008), Analysis of aircraft and satellite measurements from the Intercontinental Chemical Transport Experiment (INTEX-B) to quantify long-range transport of East Asian sulfur to Canada, *Atmospheric Chemistry and Physics*, 8, 2999-3014.

Vasilkov, A. P., Joiner, J., Oreopoulos, L., Gleason, J. F., Veefkind, P., Bucsela, E., Celarier, E. A., Spurr, R. J. D. & Platnick, S. (2009), Impact of tropospheric nitrogen dioxide on the regional radiation budget, *Atmospheric Chemistry and Physics*, 9, 6389-6400, doi:10.5194/acp-9-6389-2009.

Veefkind, J. P., Aben, I., McMullan, K., Förster, H., de Vries, J., Otter, G., Claas, J., Eskes, H. J., de Haan, J. F., Kleipool, Q., van Weele, M., Hasekamp, O., Hoogeveen, R., Landgraf, J., Snel, R., Tol, P., Ingmann, P., Voors, R., Kruizinga, B., Vink, R., Visser, H., & Levelt, P. F. (2012), TROPOMI on the ESA Sentinel-5 Precursor: A GMES mission for global observations of the atmospheric composition for climate, air quality and ozone layer applications, *Remote Sensing of Environment*, 120, 70-83.

Virts, K. S., Wallace, J. M., Hutchins, M. L., & Holzworth, R. H. (2013), Highlights of a new ground-based, hourly global lightning climatology, *Bulletin of the American Meteorological Society*, 94, 1381-1392.

Wang, Y., DeSilva, A. W., & Goldenbaum, G. C. (1998) Nitric oxide production by simulated lightning: Dependence on current, energy and pressure. *Journal of Geophysical Research: Atmospheres*, 103 (D15), 19149 – 19159.

Wenig, M., Kühl, S., Beirle, S., Bucsela, E., Jähne, B., Platt, U., Gleason, J., Wagner, T. (2003), Retrieval and analysis of stratospheric NO_2 from the Global Ozone Monitoring Experiment, *Journal of Geophysical Research: Atmospheres*, 109, D04315.

Weiss, S. A., MacGorman, D. R., & Calhoun, K. M. (2012), Lightning in the anvils of supercell thunderstorms. *Monthly Weather Review*,140, 2064–2079.

Williams, E. R. (1985), Large-scale charge separation in thunderclouds, *Journal of Geophysical Research: Atmospheres*, 90, 6013–6025.

Yang, K., S., Carn, A., Ge, C., Wang, J., & Dickerson, R. R. (2014), Advancing measurements of tropospheric NO_2 from space: New algorithm and first global results from OMPS, *Geophysical Research Letters*, 41, 4777–4786, doi:10.1002/2014GL060136.

Ziemke, JR, Chandra, S., & Bhartia, P. K. (2001), "Cloud slicing": A new technique to derive upper tropospheric ozone from satellite measurements, *Journal of Geophysical Research: Atmospheres*, 106, 9853-9868, doi: 10.1029/2000jd9008.

Ziemke, J. R., Chandra, S., Duncan, B. N., Froidevaux, L., Bhartia, P. K., Levelt, P. F., & Waters, J. W. (2006), Tropospheric ozone determined from Aura OMI and MLS: Evaluation of measurements and comparison with the Global Modeling Initiative's Chemical Transport Model, *Journal of Geophysical Research: Atmospheres*, 111, D19303, doi:10.1029/2006JD007089.

Zara, M., Boersma, K. F., De Smedt, I., Richter, A., Peters, E., Van Geffen, J. H. G. M., Beirle, S., Wagner, T., Van Roozendael, M., Marchenko, S., Lamsal, L. N., & Eskes, H. J. (2017), Improved slant column density retrieval of nitrogen dioxide and formaldehyde for OMI and GOME-2A from QA4ECV: intercomparison, uncertainty characterization, and trends, *Atmospheric Measurement Techniques*, doi 10.5194.

Zoogman, P., et al, Tropospheric emissions: Monitoring of pollution (TEMPO), *J. Quantitative Spectroscopy and Radiative Transfer*, 186, 17-39, 2017.